Physica D 415 (2021) 132768

Contents lists available at ScienceDirect

Physica D

journal homepage: www.elsevier.com/locate/physd

# Fluid vesicles with internal nematic order

Francisco Guillén-González [a,1], María Ángeles Rodríguez-Bellido [a,1], Giordano Tierra [b,*,1]

[a] Departamento de Ecuaciones Diferenciales y Análisis Numérico and IMUS, Universidad de Sevilla, Facultad de Matemáticas, Campus de Reina Mercedes, C/ Tarfia, s/n- 41012 Seville, Spain

[b] Department of Mathematics, University of North Texas, Denton, TX 76203, USA

ARTICLE INFO

*Article history:*
Received 18 March 2020
Received in revised form 31 August 2020
Accepted 10 October 2020
Available online 22 October 2020
Communicated by C. Josserand

*Keywords:*
Diffuse interface/phase field
Liquid crystals
Two phase flow
Vesicle membrane

ABSTRACT

Models of flows containing vesicles membranes with liquid crystalline phases have been widely studied in recent times due to its connection with biological applications.

In this work we propose a new model to represent the interaction between flows and vesicle membranes with internal nematic order and preferential orientation of their molecules in the membrane. In fact, the dynamics of the system is determined by the dissipation of an energy that regulates the competition between different effects, through the kinetic, bending, elastic and anchoring energies.

Moreover we introduce a new numerical scheme to approximate the model, that is unconditionally energy stable. Additionally, we present several numerical results in order to show the well behavior of the proposed scheme and the dynamics of this type of vesicle membranes.



## 1. Introduction

Vesicle membranes can be defined as closed structures made of bilayers (usually two lipid monolayers with anchored proteins) that separates an aqueous compartment from a surrounding fluid. The study of their structural changes, dynamics and deformation is presenting a growing interest due to its applications to Biology, Biophysics and Bioengineering [1–4].

In addition, these materials are coupled with environmental conditions, that might include interactions with different type of flows, thermotropic effects and electric or magnetic fields [4,5]. For instance, the dynamical behavior of fluid vesicles in various types of external hydrodynamic flow is determined by a complex interplay between membrane elasticity, hydrodynamic forces, and thermal fluctuations acting at microscopic length scales and it is fundamental for understanding the dynamics of these soft objects. We refer the reader to [6] for a nice review on these type of dynamics and to the works [7–9] for experimental and numerical studies of the motion of vesicles through constrictions.

In particular, there is a growing interest on understanding the coupling of vesicle membranes with anisotropic flows of the liquid crystal type in which they are immersed or filled. In fact, liquid crystals-type of flow play an important role in the dynamics of biological components [10–12]. For instance, in [13] it is shown that extracellular matrices of fibrous tissues in plants and animals are very similar to cholesteric liquid crystals, although it is important to keep in mind that the living cells present in those systems introduce additional difficulties to model such type of systems in an effective way. Moreover, liquid crystalline phases are found in many biological materials, such as actin, DNA, cellulose, collagen...and they can be responsible for the deformation of cell membranes [14]. There are also evidences [15] that actin and tubulin networks (both liquid crystalline materials) are capable of deforming the shape of cells until they reach an equilibrium (anisotropic shape) and the magnitude of the deformation is determined by a balance of elastic and surface forces. Moreover, active nematic film of microtubules and molecular motors encapsulated within a shape-changing lipid vesicle exhibit a myriad of dynamical states produced by a combination of activity, topological constraints and vesicle deformability [16]. Additionally, vesicles formed from block copolymers with liquid-crystalline side chains reveal a rich variety of vesicle morphologies, and the authors of Xing et al. [17] have developed a model to study the morphology of the membrane structure with internal nematic and smectic order. Furthermore, it has been shown that biological cell dynamics have intricate properties when they are immersed in nematic liquid crystals [18–20].

The shape of the vesicle membranes can be modeled by using the minimizers of different surface energies, such as the bending elastic energy, which are associated to the equilibrium shapes when vesicle membranes are not interacting with external fields. This idea together with localizing the membrane using the diffuse interface approach has been used to develop gradient flow models [21–29] that have been studied analytically and numerically

* Corresponding author.
*E-mail addresses:* guillen@us.es (F. Guillén-González), angeles@us.es (M.Á. Rodríguez-Bellido), gtierra@unt.edu (G. Tierra).

[1] The three authors contributed equally to this study.

https://doi.org/10.1016/j.physd.2020.132768
0167-2789/

with and without coupling with external fields (check [30–38] and the references therein). Moreover, these type of phase field models have shown to be very versatile in its application to cell motility [39].

This work is an extension of the work analyzed in [40], where a model to represent vesicle membranes with nematic order and taking into account anchoring effects was presented and studied. In this new approach we also include the interaction of the membrane with internal and external flows (they might be flows with different properties) to represent a more realistic setting, that leads to a richer phenomenology [6]. In fact, the ideas can be viewed as an extension of the vesicle membrane model studied in [37] (that comes from the interesting work presented in [26]). We consider a vesicle membrane containing (or immersed in) a nematic liquid crystal flow, whose orientation, its interaction with the membrane (anchoring effects) and its interaction with the surrounding flow will determine the dynamics and equilibrium configurations of the system. The coupling between the external flow and the internal liquid crystal part will be treated as a phase field system, and derived using similar arguments to the ones presented in [41], where the authors presented and studied a model for complex fluids composed by the mixture between isotropic (Newtonian fluid) and nematic (liquid crystal) flows taking into account anchoring effects of the liquid crystal molecules on the interface between both fluids.

The paper is organized as follows: We present the model that we are considering and the main ideas to derive such a model in Section 2. Then, we develop a new numerical splitting scheme over this model on Section 3. In a first step, an approximation only in space is made, which conserves the unconditional energy stability property of the continuous model. After that, a complete discrete approximation (in space and time) is developed resulting in a numerical scheme that also preserves the unconditionally energy stability property. Numerical results are presented in Section 4 to illustrate the type of dynamics that can be obtained using the proposed numerical scheme. Finally, we state the conclusions of our work in Section 5.

## 2. The model

As previously mentioned, we consider a phase field system to model the interaction between the fluid settled in the internal part of the vesicle membrane and the external one. We denote by $\phi(\boldsymbol{x}, t)$ the phase field variable which is used to localize the interior ($\phi = 1$) and the exterior ($\phi = -1$) of the membrane. The dynamics of the membrane are derived through the energetic variational approach with respect to the total energy ($E_{tot}(\boldsymbol{u}, \phi, \boldsymbol{d})$) of the system, that relates the kinetic, bending, nematic and anchoring energies.

The bending energy is the energy stored in the vesicle membrane shape, and usually is represented by using the Helfrich bending energy:

$$\mathcal{H}(\Gamma) = \kappa_0 \int_\Gamma \frac{1}{2}\left(H(\boldsymbol{x}) - k(\boldsymbol{x})\right)^2 d\sigma(\boldsymbol{x}) + \bar{\kappa} \int_\Gamma K(\boldsymbol{x}) d\sigma(\boldsymbol{x}),$$

being $\Gamma \subset \mathbb{R}^3$ a smooth, compact surface without boundary representing the membrane of the vesicle (the domain occupied by the whole vesicle will be denoted by $\Omega$), $d\sigma(\boldsymbol{x})$ the surface differential, $\kappa_0$ and $\bar{\kappa}$ two bending rigidity coefficients and $k(\boldsymbol{x})$ a given function representing the spontaneous curvature. Functions $H(\boldsymbol{x}) = k_1(\boldsymbol{x}) + k_2(\boldsymbol{x})$ and $K(\boldsymbol{x}) = k_1(\boldsymbol{x}) \cdot k_2(\boldsymbol{x})$ are defined using $k_1(\boldsymbol{x})$ and $k_2(\boldsymbol{x})$ the principles curvatures at each point $\boldsymbol{x}$.

In this work, we consider a bounded domain $\Omega \subset \boldsymbol{R}^M (M = 2, 3)$, whose boundary will be represented by $\partial\Omega$. We replace the Helfrich energy equation by the bending energy associated to a phase field function used to localize the membrane. In particular, we follow the approach presented in [26,42] where the bending energy is consistent with the general framework of the energetic variational approach (EVA), takes into account the spontaneous curvature of the membrane and converges to the Helfrich one when $\varepsilon \to 0$ [43], where $\varepsilon > 0$ is a parameter related with the interfacial width of the vesicle membrane. The bending energy considered along this paper is defined as

$$E_{ben}(\phi) := \frac{\varepsilon}{2}\int_\Omega \left(\Delta\phi - \frac{1}{\varepsilon^2}G(\phi)\right)^2 d\boldsymbol{x} = \frac{\varepsilon}{2}\int_\Omega \omega^2 d\boldsymbol{x}, \tag{2.1}$$

where

$$\omega := -\Delta\phi + \frac{1}{\varepsilon^2}G(\phi), \qquad G(\phi) := F'(\phi) - \varepsilon k(\boldsymbol{x}) H'(\phi) \tag{2.2}$$

with

$$F(\phi) := \frac{1}{4}(\phi^2 - 1)^2, \quad H(\phi) := \frac{1}{3}\phi^3 - \phi,$$

being $F(\phi)$ the Ginzburg–Landau potential, $k(\boldsymbol{x})$ a given function representing the spontaneous curvature and $H(\phi)$ a function that appears when the spontaneous curvature is considered. The volume and surface area of the vesicle are defined as

$$\begin{aligned} V(\phi) &:= \frac{1}{2}\int_\Omega (\phi + 1)\, d\boldsymbol{x} \quad \text{and} \\ B(\phi) &:= \int_\Omega \left(\frac{\varepsilon}{2}|\nabla\phi|^2 + \frac{1}{\varepsilon}F(\phi)\right) d\boldsymbol{x}, \end{aligned} \tag{2.3}$$

respectively. We want to develop a model such that the volume and surface area of the vesicles remain constant in time, that is, we need to enforce somehow these constraints in our model. In particular, instead of enforcing directly that the volume remains constant in time, we will enforce that $A(\phi)$ remains constant, where

$$A(\phi) := \int_\Omega \phi\, d\boldsymbol{x},$$

because the two constraints are equivalent. We are going to follow the approach considered in [37,40], where the volume conservation is enforced exactly by taking a $H^{-1}$-gradient flow (by using a Cahn–Hilliard-type model which directly enforce the volume conservation property) while the conservation of the surface area will be approximated by introducing a penalization term in the bending energy. In particular, the energy terms read:

$$E_{bp}(\phi) := E_{ben}(\phi) + \frac{1}{2\eta}\left(B(\phi) - \beta\right)^2, \tag{2.4}$$

with $E_{ben}(\phi)$ defined in (2.1), $\eta > 0$ being the penalization parameter, $B(\phi)$ the surface area of the vesicle given in (2.3) and $\beta > 0$ the desired surface area of the system.

Let $\boldsymbol{u}(\boldsymbol{x}, t)$ be the fluid velocity field (internal or external to the vesicle membrane) and $\boldsymbol{d}(\boldsymbol{x}, t)$ the mean director vector of the liquid crystal molecules. The total energy of the considered system is:

$$E_{tot}(\boldsymbol{u}, \phi, \boldsymbol{d}) = E_{kin}(\boldsymbol{u}) + \lambda_{bp}E_{bp}(\phi) + \lambda_{nem}E_{nem}(\boldsymbol{d}, \phi) + \lambda_{anch}\, E_{anch}(\boldsymbol{d}, \phi), \tag{2.5}$$

where $E_{kin}(\boldsymbol{u}) = \frac{1}{2}\int_\Omega |\boldsymbol{u}|^2\, d\boldsymbol{x}$ denotes the kinetic energy associated to the fluid velocity $\boldsymbol{u}$, $E_{bp}(\phi)$ the penalized bending energy given in (2.4), $E_{nem}(\boldsymbol{d}, \phi)$ the elastic energy due to the nematic liquid crystal (that also contains a penalization part related to the unitary constraint of the director vector $|\boldsymbol{d}| = 1$) and $E_{anch}(\boldsymbol{d}, \phi)$ the anchoring energy that represents the influence of the interfacial effects on the orientation of the nematic liquid crystal molecules on the surface of the membrane. Positive parameters $\lambda_{bp}$, $\lambda_{nem}$ and $\lambda_{anch}$ are introduced to balance the effect of each

energy in the system. On the other hand, the nematic energy is described as

$$E_{nem}(\boldsymbol{d},\phi) := \int_\Omega I(\phi)\left(\frac{1}{2}|\nabla \boldsymbol{d}|^2 + P(\boldsymbol{d})\right) d\boldsymbol{x},$$

where the function $P(\boldsymbol{d})$ (whose derivative will be denoted as $\boldsymbol{p}(\boldsymbol{d}) := P'(\boldsymbol{d})$) is defined as the following double-well potential whose minimums (and consequently their equilibrium states) are located at $|\boldsymbol{d}| = 1$:

$$P(\boldsymbol{d}) := \frac{1}{4\eta_{\boldsymbol{d}}^2}(|\boldsymbol{d}|^2 - 1)^2,$$

with $\eta_{\boldsymbol{d}} > 0$ being a penalization parameter. The volume fraction of the liquid crystal will be denoted by $I(\phi)$ ($I(\phi) \in [0,1]$) and we will consider that it takes the same form previously introduced in [40,41], with its derivative denoted by $i(\phi) := I'(\phi)$. This function $I(\phi)$ is introduced in order to being able to define the nematic energy globally in the whole domain $\Omega$, but vanishing in the newtonian part, being equal to one in the liquid crystal part, and a regular intermediate function over the membrane (matching the newtonian and the nematic part). Concretely, the volume fraction $I(\phi)$ is defined as follows:

$$I(\phi) := \begin{cases} \frac{1}{16}(\phi+1)^3(3\phi^2 - 9\phi + 8) & \text{if } \phi \in (-1,1), \\ 1 & \text{if } \phi \geq 1, \\ 0 & \text{if } \phi \leq -1, \end{cases}$$

whose derivative is given by

$$i(\phi) := I'(\phi) = \begin{cases} \frac{15}{16}(\phi+1)^2(\phi-1)^2 & \text{if } \phi \in (-1,1), \\ 0 & \text{in other case}. \end{cases}$$

Finally, the anchoring energy has the form:

$$E_{anch}(\boldsymbol{d},\phi) := \frac{1}{2}\int_\Omega \left(\delta_1|\boldsymbol{d}|^2|\nabla\phi|^2 + \delta_2|\boldsymbol{d}\cdot\nabla\phi|^2\right) d\boldsymbol{x},$$

with $(\delta_1,\delta_2)$ depending on the anchoring effect considered:

$$(\delta_1,\delta_2) = \begin{cases} (0,0) & \text{No anchoring}, \\ (0,1) & \text{Parallel anch.}, \\ (1,-1) & \text{Homeotropic anch.}. \end{cases} \tag{2.6}$$

Observe that the anchoring energy is defined in the whole domain $\Omega$ but it only acts on the membrane, because $\nabla\phi \approx 0$ inside and outside the membrane.

Now, we are going to derive the coupled system, considering it as a thermodynamically consistent complex fluid composed by two different fluids separated by a elastic interface of a certain width (in this case the vesicle membrane). Our approach is based on using the energetic variational framework (see [44,45] for details), which has proved itself useful to design thermodynamically consistent models in several applications such as liquid crystals, mixtures of fluids, biofilms or blood clots, to name a few [46–49]. This can be done combining ideas from the Least Action Principle (LAP) and the Maximum Dissipation Principle (MDP), arriving at the following PDE system:

$$\begin{cases} \boldsymbol{u}_t + (\boldsymbol{u}\cdot\nabla)\boldsymbol{u} + \nabla p - \nabla\cdot\boldsymbol{\sigma}_{tot} = \boldsymbol{0}, \\ \nabla\cdot\boldsymbol{u} = 0, \\ \boldsymbol{d}_t + (\boldsymbol{u}\cdot\nabla)\boldsymbol{d} + \gamma_{nem}\left(\frac{\delta E_{tot}}{\delta \boldsymbol{d}}\right) = \boldsymbol{0}, \\ \phi_t + (\boldsymbol{u}\cdot\nabla)\phi - \nabla\cdot\left(\gamma_{ben}\nabla\frac{\delta E_{tot}}{\delta\phi}\right) = 0. \end{cases} \tag{2.7}$$

The expressions for each variational derivative in (2.7) will be introduced as two new variables:

$$\begin{aligned} \boldsymbol{z} := \frac{\delta E_{tot}}{\delta \boldsymbol{d}} &= \lambda_{nem}\frac{\delta E_{nem}}{\delta \boldsymbol{d}} + \lambda_{anch}\frac{\delta E_{anch}}{\delta \boldsymbol{d}} \\ &= \lambda_{nem}\Big(-\nabla\cdot(I(\phi)\nabla\boldsymbol{d}) + I(\phi)\boldsymbol{p}(\boldsymbol{d})\Big) + \lambda_{anch}\frac{\delta E_{anch}}{\delta \boldsymbol{d}}, \end{aligned}$$

and

$$\begin{aligned} \mu := \frac{\delta E_{tot}}{\delta\phi} &= \lambda_{bp}\frac{\delta E_{bp}}{\delta\phi} + \lambda_{nem}\frac{\delta E_{nem}}{\delta\phi} + \lambda_{anch}\frac{\delta E_{anch}}{\delta\phi} \\ &= \lambda_{bp}\left(-\varepsilon\,\Delta\omega + \frac{1}{\varepsilon}G'(\phi)\,\omega \right. \\ &\quad \left. + \frac{1}{\eta}(B(\phi)-\beta)\Big(-\varepsilon\Delta\phi + \frac{1}{\varepsilon}F'(\phi)\Big)\right) \\ &\quad + \lambda_{nem}I'(\phi)\left(\frac{1}{2}|\nabla\boldsymbol{d}|^2 + P(\boldsymbol{d})\right) + \lambda_{anch}\frac{\delta E_{anch}}{\delta\phi}, \end{aligned}$$

where the anchoring terms will depend on the case considered ($(\delta_1,\delta_2)$ as in (2.6)):

$$\frac{\delta E_{anch}}{\delta \boldsymbol{d}} = \delta_1|\nabla\phi|^2\boldsymbol{d} + \delta_2(\boldsymbol{d}\cdot\nabla\phi)\nabla\phi, \tag{2.8}$$

and

$$\frac{\delta E_{anch}}{\delta\phi} = \nabla\cdot\left(\delta_1|\boldsymbol{d}|^2\nabla\phi + \delta_2(\boldsymbol{d}\cdot\nabla\phi)\boldsymbol{d}\right). \tag{2.9}$$

Finally, the stress tensor of the coupled system (2.7) reads:

$$\boldsymbol{\sigma}_{tot} = \boldsymbol{\sigma}_{vis} + \boldsymbol{\sigma}_{bp} + \boldsymbol{\sigma}_{nem} + \boldsymbol{\sigma}_{anch},$$

where

$$\begin{aligned} \boldsymbol{\sigma}_{vis} &= 2\,\nu(\phi)\boldsymbol{D}\boldsymbol{u}, \\ \boldsymbol{\sigma}_{bp} &= \boldsymbol{\sigma}_b + \boldsymbol{\sigma}_p = \lambda_{bp}\,\varepsilon\Big[-\nabla\phi\otimes\nabla\omega + (\nabla^2\phi)\,\omega \\ &\quad -\frac{1}{\eta}\big(B(\phi)-\beta\big)(\nabla\phi\otimes\nabla\phi)\Big], \\ \boldsymbol{\sigma}_{nem} &= -\lambda_{nem}I(\phi)(\nabla\boldsymbol{d})^t\nabla\boldsymbol{d}, \end{aligned}$$

(recall that $\omega$ was introduced in (2.2)) and

$$(\boldsymbol{\sigma}_{anch})_{ij} = \lambda_{anch}\begin{cases} 0 & \text{No anchoring}, \\ -(\boldsymbol{d}\cdot\nabla\phi)\,(\nabla\phi\otimes\boldsymbol{d}) & \text{Parallel anch.}, \\ -|\boldsymbol{d}|^2\,\nabla\phi\otimes\nabla\phi + (\boldsymbol{d}\cdot\nabla\phi)\,(\nabla\phi\otimes\boldsymbol{d}) & \text{Homeotropic anch.}. \end{cases}$$

Hereafter, $\otimes$ denotes the tensorial product, for instance $(\nabla\phi\otimes\boldsymbol{d})_{ij} = \partial_i\phi\,d_j$.

Observe that (2.7) is a highly nonlinear system: there are convective terms ($(\boldsymbol{u}\cdot\nabla)\boldsymbol{u}$, $(\boldsymbol{u}\cdot\nabla)\boldsymbol{d}$ and $(\boldsymbol{u}\cdot\nabla)\phi$), and most of the terms involved on the variational derivatives of the energy ($\frac{\delta E_{tot}}{\delta\boldsymbol{d}}$ and $\frac{\delta E_{tot}}{\delta\phi}$) and of the tensor $\boldsymbol{\sigma}_{tot}$ are also nonlinear terms. The highly nonlinear character of the system requires a suitable (non-trivial) numerical approximation in order to catch the main features of the continuous model.

**Remark 2.1.** Since the viscosities of each component of the mixture could be different, in order to simplify, we have considered the viscosity coefficient $\nu$ depending on the phase function $\phi$, where $\nu(\phi)$ is a strictly positive function such that $\nu(-1) = \nu_{Nw}$ (the viscosity of the newtonian fluid) and $\nu(1) = \nu_{Lc}$ (the viscosity of the nematic liquid crystal)

The effect of the stress tensor $-\nabla\cdot\boldsymbol{\sigma}_{tot}$ can be rewritten in order to arrive at a simpler formulation of the model, where these new terms are going to be easier to handle.

**Lemma 2.2** (*Reformulation of the Stress Tensor*)**.** *It holds:*

$$-\nabla\cdot\boldsymbol{\sigma}_{bp}-\nabla\cdot\boldsymbol{\sigma}_{nem}-\nabla\cdot\boldsymbol{\sigma}_{anch}=-\mu\,\nabla\phi-(\nabla\boldsymbol{d})^t\boldsymbol{z}+\nabla\varphi,$$

*where*

$$\begin{aligned}\varphi &= \lambda_{nem}\,I(\phi)\left(\frac{1}{2}\,|\nabla\boldsymbol{d}|^2+P(\boldsymbol{d})\right)\\ &+ \lambda_{bp}\left(\frac{\varepsilon}{2}\,\omega^2+\frac{1}{\eta}\big(B(\phi)-\beta\big)\left(\frac{\varepsilon}{2}|\nabla\phi|^2+\frac{1}{\varepsilon}F(\phi)\right)\right)\\ &+ \frac{\lambda_{anch}}{2}\,W(\boldsymbol{d},\phi),\end{aligned}$$

*and*

$$W(\boldsymbol{d},\phi)=\begin{cases}0 & \textit{No anchoring},\\ |\boldsymbol{d}\cdot\nabla\phi|^2 & \textit{Parallel anch.},\\ \big(|\boldsymbol{d}|^2\,|\nabla\phi|^2-|\boldsymbol{d}\cdot\nabla\phi|^2\big) & \textit{Homeotropic anch.}.\end{cases}$$

**Proof.** We focus on the terms related with $\nabla\cdot\boldsymbol{\sigma}_{bp}$, due to the fact that the rest of the operations are equivalent to the ones presented in [41].

Decomposing the purely bending part and the penalized one as follows

$$\begin{aligned}\mu_{bp}&=\mu_b+\mu_p=\lambda_{bp}\left(-\varepsilon\,\Delta\omega+\frac{1}{\varepsilon}G'(\phi)\,\omega\right)\\ &+\lambda_{bp}\frac{1}{\eta}(B(\phi)-\beta)\left(-\varepsilon\Delta\phi+\frac{1}{\varepsilon}F'(\phi)\right)\\ \varphi_{bp}&=\varphi_b+\varphi_p=\lambda_{bp}\left(\frac{\varepsilon}{2}\,\omega^2\right)+\lambda_{bp}\,\frac{1}{\eta}\\ &\times\big(B(\phi)-\beta\big)\left(\frac{\varepsilon}{2}|\nabla\phi|^2+\frac{1}{\varepsilon}F(\phi)\right).\\ \boldsymbol{\sigma}_{bp}&=\boldsymbol{\sigma}_b+\boldsymbol{\sigma}_p=\lambda_{bp}\,\varepsilon\Big(-\nabla\phi\otimes\nabla\omega+(\nabla^2\phi)\,\omega\Big)\\ &-\lambda_{bp}\,\varepsilon\frac{1}{\eta}\big(B(\phi)-\beta\big)\,(\nabla\phi\otimes\nabla\phi),\end{aligned}$$

it suffices to prove that

$$\nabla\cdot\boldsymbol{\sigma}_b=\mu_b\,\nabla\phi-\nabla\varphi_b\quad\text{and}\quad\nabla\cdot\boldsymbol{\sigma}_p=\mu_p\,\nabla\phi-\nabla\varphi_p.$$

First we check the purely bending part and after the penalized one. Indeed, on the one hand

$$(\nabla\cdot(\nabla\phi\otimes\nabla\omega))_i=\partial_i\phi\,\Delta\omega+\partial_{ij}\phi\,\partial_j\omega=\partial_i\phi\,\Delta\omega+\partial_j(\partial_{ij}\phi\,\omega)-\Delta\partial_i\phi\,\omega,$$

hence

$$\nabla\cdot\boldsymbol{\sigma}_b=\lambda_{bp}\,\varepsilon\nabla\cdot(-\nabla\phi\otimes\nabla\omega+(\nabla^2\phi)\,\omega)=\lambda_{bp}\,\varepsilon(-\nabla\phi\,\Delta\omega+\Delta\nabla\phi\,\omega)$$

and on the other hand

$$\begin{aligned}&\mu_b\,\nabla\phi-\nabla\varphi_b=\lambda_{bp}\left(-\varepsilon\,\Delta\omega+\frac{1}{\varepsilon}G'(\phi)\,\omega\right)\,\nabla\phi-\lambda_{bp}\,\nabla\left(\frac{\varepsilon}{2}\,\omega^2\right)\\ &=\lambda_{bp}\left(-\varepsilon\,\Delta\omega+\frac{1}{\varepsilon}G'(\phi)\,\omega\right)\,\nabla\phi-\lambda_{bp}\varepsilon\,\omega\left(-\Delta\nabla\phi+\frac{1}{\varepsilon^2}G'(\phi)\nabla\phi\right)\\ &=\lambda_{bp}\,\varepsilon(-\nabla\phi\,\Delta\omega+\Delta\nabla\phi\,\omega).\end{aligned}$$

Consequently, one has the equality $\nabla\cdot\boldsymbol{\sigma}_b=\mu_b\,\nabla\phi-\nabla\varphi_b$.

In order to prove $\nabla\cdot\boldsymbol{\sigma}_p=\mu_p\,\nabla\phi-\nabla\varphi_p$ we follow the following computations

$$\begin{aligned}(\mu_p\,\nabla\phi-\nabla\varphi_p)_i&=\lambda_{bp}\frac{1}{\eta}(B(\phi)-\beta)\left(-\varepsilon\Delta\phi+\frac{1}{\varepsilon}F'(\phi)\right)\,\partial_i\phi\\ &-\lambda_{bp}\,\frac{1}{\eta}\big(B(\phi)-\beta\big)\partial_i\left(\frac{\varepsilon}{2}|\nabla\phi|^2+\frac{1}{\varepsilon}F(\phi)\right)\\ &=\lambda_{bp}\frac{1}{\eta}(B(\phi)-\beta)\left[\left(-\varepsilon\,\Delta\phi+\frac{1}{\varepsilon}F'(\phi)\right)\,\partial_i\phi\right.\\ &\left.-\left(\varepsilon\nabla\phi\cdot\nabla\partial_i\phi\;+\frac{1}{\varepsilon}F'(\phi)\partial_i\phi\right)\right]\\ &=\lambda_{bp}\varepsilon\frac{1}{\eta}(B(\phi)-\beta)\big[-\Delta\phi\,\partial_i\phi-\partial_j(\partial_i\phi\,\partial_j\phi)+\Delta\phi\,\partial_i\phi\big]\\ &=\lambda_{bp}\varepsilon\frac{1}{\eta}(B(\phi)-\beta)(\nabla\cdot(\nabla\phi\otimes\nabla\phi))_i.\end{aligned}$$

Thence the equality $\nabla\cdot\boldsymbol{\sigma}_p=\mu_p\,\nabla\phi-\nabla\varphi_p$ holds. ■

By applying Lemma 2.2, using the variational derivative variables $\boldsymbol{z}$ and $\mu$, and taking into account the following relations (to assure the conservation of volume of the numerical schemes):

$$\begin{cases}\mu\nabla\phi=\nabla(\phi\mu)-\phi\nabla\mu\,,\\ \boldsymbol{u}\cdot\nabla\phi=\nabla\cdot(\phi\,\boldsymbol{u}),\end{cases}$$

system (2.7) can be reformulated as:

$$\begin{cases}\boldsymbol{u}_t+\boldsymbol{u}\cdot\nabla\boldsymbol{u}+\nabla\widetilde{p}-\nabla\cdot(2\nu(\phi)\boldsymbol{D}\boldsymbol{u})+\phi\,\nabla\mu-(\nabla\boldsymbol{d})^t\boldsymbol{z} &= \boldsymbol{0},\\ \nabla\cdot\boldsymbol{u} &= 0,\\ \boldsymbol{d}_t+(\boldsymbol{u}\cdot\nabla)\boldsymbol{d}+\gamma_{nem}\boldsymbol{z} &= \boldsymbol{0},\\ \lambda_{nem}[-\nabla\cdot(I(\phi)\nabla\boldsymbol{d})+I(\phi)\,\boldsymbol{p}(\boldsymbol{d})]+\lambda_{anch}\,\dfrac{\delta E_{anch}}{\delta\boldsymbol{d}}-\boldsymbol{z} &= \boldsymbol{0},\\ \phi_t+\nabla\cdot(\phi\,\boldsymbol{u})-\nabla\cdot(\gamma_{ben}\nabla\mu) &= 0,\\ \lambda_{bp}\left(-\varepsilon\,\Delta\omega+\dfrac{1}{\varepsilon}G'(\phi)\omega+\dfrac{1}{\eta}(B(\phi)-\beta)\Big(-\varepsilon\Delta\phi+\dfrac{1}{\varepsilon}F'(\phi)\Big)\right)&\\ +\lambda_{nem}I'(\phi)\left(\dfrac{1}{2}|\nabla\boldsymbol{d}|^2+P(\boldsymbol{d})\right)+\lambda_{anch}\,\dfrac{\delta E_{anch}}{\delta\phi}-\mu &= 0,\\ \varepsilon\omega+\varepsilon\Delta\phi-\dfrac{1}{\varepsilon}G(\phi) &= 0,\end{cases}\tag{2.10}$$

where $(\delta E_{anch}/\delta\boldsymbol{d})$ and $(\delta E_{anch}/\delta\phi)$ were previously defined in (2.8) and (2.9) respectively, $\gamma_{nem},\gamma_{ben}>0$ are time relaxation parameters and the following modified potential appears:

$$\widetilde{p}:=p+\varphi-\phi\,\mu.$$

The first two equations in the nonlinear coupled system (2.10) are devoted to the movement of the fluid, and apart of the effects included in the standard Navier–Stokes system, they also includes the contribution of the nematic liquid crystal and the vesicle membrane to the dynamics of the fluid through the terms $(\nabla\boldsymbol{d})^t\boldsymbol{z}$ and $\phi\,\nabla\mu$, respectively. The third and fourth equations represent the dynamics of the nematic liquid crystal part (remember that $\boldsymbol{d}$ represents the orientation of the average orientation of the nematic molecules) and it includes nonlinear transport effects due to the fluid velocity $\boldsymbol{u}$ and nonlinear interactions with the phase field unknown through the volume fraction $I(\phi)$ and the anchoring effects. Finally, the last three equations in (2.10) are devoted to the dynamics of the vesicle membrane and they include nonlinear transport effects due to the fluid velocity $\boldsymbol{u}$, a global nonlinearity related with the penalization of the conservation of surface constraint (the term $(1/\eta)(B(\phi)-\beta)(-\varepsilon\Delta\phi+(1/\varepsilon)F'(\phi))$) and nonlinear contributions of the liquid crystal to the dynamics of the vesicle.

The PDE system (2.10) is supplemented with the following initial and boundary conditions:

$$\begin{aligned} &\boldsymbol{u}|_{t=0}= \boldsymbol{u}_0, \quad \boldsymbol{d}|_{t=0}= \boldsymbol{d}_0, \quad \phi|_{t=0}= \phi_0 && \text{in } \Omega,\\ &\boldsymbol{u}|_{\partial\Omega}= \big(I(\phi)\nabla \boldsymbol{d}\big)\cdot \boldsymbol{n}\big|_{\partial\Omega} = \boldsymbol{0}, \quad \nabla\mu\cdot\boldsymbol{n}|_{\partial\Omega}= 0 && \text{in } (0,T),\\ &\phi|_{\partial\Omega}= -1\,, \quad \nabla\phi\cdot\boldsymbol{n}|_{\partial\Omega}= 0\,, && \text{in } (0,T), \end{aligned} \tag{2.11}$$

where $\boldsymbol{n}$ denotes the outwards normal vector to the boundary $\partial\Omega$, and $T > 0$ will be the final time observed for the solution of the system (2.10)–(2.11). Following the phenomenological derivation of the model, the boundary conditions have been taken in such a way that starting from (2.10)–(2.11) and considering adequate test functions the energy law (2.12) can be obtained.

**Lemma 2.3.** *Problem (2.10)–(2.11) satisfies the following dissipative energy law,*

$$\begin{aligned} &\frac{d}{dt}\widetilde{E}_{tot}(\boldsymbol{u}(t),\phi(t),\boldsymbol{d}(t),\omega(t)) + \left\|\sqrt{2\nu(\phi(t))}\nabla\boldsymbol{u}(t)\right\|^2_{L^2}\\ &\quad + \gamma_{ben}\,\|\nabla\mu(t)\|^2_{L^2} + \gamma_{nem}\,\|\boldsymbol{z}(t)\|^2_{L^2} = 0\,, \end{aligned} \tag{2.12}$$

*where the following modified energy appears*

$$\begin{aligned} \widetilde{E}_{tot}(\boldsymbol{u},\phi,\boldsymbol{d},\omega) \,=\, & E_{kin}(\boldsymbol{u}) + \lambda_{bp}\widetilde{E}_{bp}(\phi,\omega) + \lambda_{nem}E_{nem}(\boldsymbol{d},\phi)\\ & + \lambda_{anch}\,E_{anch}(\boldsymbol{d},\phi), \end{aligned}$$

*with*

$$\widetilde{E}_{bp}(\phi,\omega) \,=\, \frac{\varepsilon}{2}\int_\Omega \omega^2 d\boldsymbol{x} \,+\, \frac{1}{2\eta}\big(B(\phi)-\beta\big)^2.$$

**Proof.** Testing $(2.10)_1$ by $\boldsymbol{u}$, $(2.10)_2$ by $p$, $(2.10)_3$ by $\boldsymbol{z}$, $(2.10)_4$ by $\boldsymbol{d}_t$ $(2.10)_5$ by $\mu$, $(2.10)_6$ by $\phi_t$ and $((2.10)_7)_t$ by $\lambda_{bp}\omega$, and adding these relations we easily derive the energy law (2.12). ■

## 3. Numerical scheme

The aim of this section is to design unconditionally energy-stable schemes for approximating system (2.10), that is, we focus on designing numerical schemes that satisfy a dissipative energy law, similar to (2.12), without imposing restrictions over the discrete parameters involved.

### 3.1. A generic FE space-discrete scheme

Let

$$\begin{aligned} &\boldsymbol{V}_h\times P_h\times \boldsymbol{D}_h\times \boldsymbol{Z}_h\times \Phi_h\times M_h\times W_h \subset \boldsymbol{H}^1_0(\Omega)\times L^2_0(\Omega)\times \boldsymbol{H}^1(\Omega)\\ &\quad\times \boldsymbol{L}^2(\Omega)\times H^1(\Omega)\times H^1(\Omega)\times H^1(\Omega) \end{aligned}$$

be conformed finite element spaces associated to a regular and quasi-uniform triangulation $\mathcal{T}_h$ of the domain $\Omega$ whose polyhedric boundary is denoted by $\partial\Omega$. Hereafter $(\cdot,\cdot)$ denotes the $L^2(\Omega)$-scalar product. For the sake of simplicity we skip the use of the subscript $h$ to denote functions that are discrete in space.

Then the Finite Element approximation of problem (2.10) reads: Find

$$\begin{aligned} &(\boldsymbol{u}(t),p(t),\boldsymbol{d}(t),\boldsymbol{z}(t),\phi(t),\mu(t),\omega(t))\in \boldsymbol{V}_h\times P_h\\ &\times \boldsymbol{D}_h\times \boldsymbol{Z}_h\times \Phi_h\times M_h\times W_h \end{aligned}$$

such that

$$\boldsymbol{u}\big|_{t=0} \,=\, P_{\boldsymbol{U}_h}\boldsymbol{u}_0\,, \quad \boldsymbol{d}\big|_{t=0} \,=\, P_{\boldsymbol{D}_h}\boldsymbol{d}_0\,, \quad \phi\big|_{t=0} \,=\, P_{\Phi_h}\phi_0\,, \quad \text{in } \Omega\,, \tag{3.13}$$

(with $P_X$ denoting the $L^2$-projection into the space $X$) and

$$\left\{\begin{aligned} \big(\boldsymbol{u}_t,\bar{\boldsymbol{u}}\big) + c(\boldsymbol{u},\boldsymbol{u},\bar{\boldsymbol{u}}) + (\nabla p,\bar{\boldsymbol{u}})&\\ +2\big(\nu(\phi)\boldsymbol{D}\boldsymbol{u},\bar{\boldsymbol{D}}\bar{\boldsymbol{u}}\big) + (\phi\,\nabla\mu,\bar{\boldsymbol{u}}) - \big((\nabla\boldsymbol{d})^t\boldsymbol{z},\bar{\boldsymbol{u}}\big) &= 0\,,\\ (\nabla\cdot\boldsymbol{u},\bar{p}) &= 0\,,\\ \big(\boldsymbol{d}_t,\bar{\boldsymbol{z}}\big) + \big((\boldsymbol{u}\cdot\nabla)\boldsymbol{d},\bar{\boldsymbol{z}}\big) + \gamma_{nem}(\boldsymbol{z},\bar{\boldsymbol{z}}) &= 0\,,\\ \lambda_{nem}\big(I(\phi)\nabla\boldsymbol{d},\nabla\bar{\boldsymbol{d}}\big) + \lambda_{nem}\big(I(\phi)\boldsymbol{p}(\boldsymbol{d}),\bar{\boldsymbol{d}}\big)&\\ +\lambda_{anch}\left(\frac{\delta E_{anch}}{\delta\boldsymbol{d}},\bar{\boldsymbol{d}}\right) - (\boldsymbol{z},\bar{\boldsymbol{d}}) &= 0\,,\\ \big(\phi_t,\bar{\mu}\big) - (\phi\,\boldsymbol{u},\nabla\bar{\mu}) + \gamma_{ben}\,(\nabla\mu,\nabla\bar{\mu}) &= 0\,,\\ \lambda_{bp}\left(\varepsilon\,(\nabla\omega,\nabla\bar{\phi}) + \frac{1}{\varepsilon}\big(G'(\phi)\omega,\bar{\phi}\big)\right)&\\ +\frac{\lambda_{bp}}{\eta}(B(\phi)-\beta)\left(\varepsilon(\nabla\phi,\nabla\bar{\phi}) + \frac{1}{\varepsilon}(F'(\phi),\bar{\phi})\right)&\\ +\lambda_{nem}\left(i(\phi)\big(\frac{1}{2}|\nabla\boldsymbol{d}|^2 + P(\boldsymbol{d})\big),\bar{\phi}\right)&\\ +\lambda_{anch}\left(\frac{\delta E_{anch}}{\delta\phi},\bar{\phi}\right) - (\mu,\bar{\phi}) &= 0\,,\\ \varepsilon(\omega,\bar{\omega}) - \varepsilon(\nabla\phi,\nabla\bar{\omega}) - \frac{1}{\varepsilon}\big(G(\phi),\bar{\omega}\big) &= 0\,, \end{aligned}\right. \tag{3.14}$$

for any

$$(\bar{\boldsymbol{u}},\bar{p},\bar{\boldsymbol{d}},\bar{\boldsymbol{z}},\bar{\phi},\bar{\mu},\bar{\omega})\in \boldsymbol{V}_h\times P_h\times \boldsymbol{D}_h\times \boldsymbol{Z}_h\times \Phi_h\times M_h\times W_h,$$

with $c(\cdot,\cdot,\cdot)$ being the trilinear antisymmetric form defined as

$$c(\boldsymbol{u},\boldsymbol{v},\boldsymbol{w}) := \Big((\boldsymbol{u}\cdot\nabla)\boldsymbol{v},\boldsymbol{w}\Big) + \frac{1}{2}\Big((\nabla\cdot\boldsymbol{u})\boldsymbol{v},\boldsymbol{w}\Big) \quad \forall\,\boldsymbol{u},\,\boldsymbol{v},\,\boldsymbol{w}\in\boldsymbol{U}_h\,. \tag{3.15}$$

We assume that the following *inf–sup* stability condition for the discrete velocity–pressure spaces $(\boldsymbol{U}_h,P_h)$ holds :

$$\sup_{\boldsymbol{u}\in\boldsymbol{U}_h\setminus\{0\}}\frac{(p,\nabla\cdot\boldsymbol{u})}{\|\boldsymbol{u}\|_{\boldsymbol{H}^1_0}} \geq \beta\|p\|_{L^2} \quad \forall\, p\in P_h\,. \tag{3.16}$$

There are many choices of $(\boldsymbol{U}_h,P_h)$ that satisfy condition (3.16), for instance the pair $(\boldsymbol{U}_h,P_h)$ can be considered either as the mini-element $((\mathbb{P}_1-bubble)\times\mathbb{P}_1)$ or the Taylor–Hood element $(\mathbb{P}_2\times\mathbb{P}_1)$ [50]. Moreover, since there are no constraints for the choices of $(\boldsymbol{D}_h,\boldsymbol{Z}_h,\Phi_h,M_h,W_h)$, we can define this set for instance considering $\mathbb{P}_1\times\mathbb{P}_1\times\mathbb{P}_1\times\mathbb{P}_1\times\mathbb{P}_1$.

**Lemma 3.1.** *Any solution $(\boldsymbol{d}(t),\boldsymbol{z}(t),\phi(t),\mu(t),\omega(t))$ of the space-discrete scheme (3.14) satisfies the following space-discrete version of the energy law (2.12):*

$$\begin{aligned} &\frac{d}{dt}\widetilde{E}_{tot}(\boldsymbol{u}(t),\phi(t),\boldsymbol{d}(t),\omega(t)) + \left\|\sqrt{2\nu(\phi(t))}\nabla\boldsymbol{u}(t)\right\|^2_{L^2}\\ &\quad + \gamma_{ben}\,\|\nabla\mu(t)\|^2_{L^2} + \gamma_{nem}\,\|\boldsymbol{z}(t)\|^2_{L^2} = 0\,. \end{aligned} \tag{3.17}$$

**Proof.** Taking in (3.14) as test functions

$$(\bar{\boldsymbol{u}},\bar{p},\bar{\boldsymbol{z}},\bar{\boldsymbol{d}},\bar{\mu},\bar{\phi}) = (\boldsymbol{u}(t),p(t),\boldsymbol{z}(t),\boldsymbol{d}_t(t),\mu(t),\phi_t(t))$$

adding with $((3.14)_7)_t$ by $\lambda_{bp}\omega$, and using the antisymmetric property

$$c(\boldsymbol{u}(t),\boldsymbol{u}(t),\boldsymbol{u}(t)) = 0,$$

we arrive at (3.17). ■

### 3.2. Fully discrete scheme

In this section we present a fully discrete numerical scheme to approximate the nonlinear problem (2.10), discretizing in time the nonlinear FE space-discrete problem presented in (3.14). For simplicity, we assume a uniform partition of the time interval $[0,T]$: $t_n = n\Delta t$, with $\Delta t = T/N$ denoting the time step, $\delta_t$ denoting the discrete time derivative and $a^{n+\frac{1}{2}}$ denoting the midpoint approximation:

$$\delta_t a^{n+1} := \frac{a^{n+1}-a^n}{\Delta t} \quad \text{and} \quad a^{n+\frac{1}{2}} := \frac{a^{n+1}+a^n}{2}.$$

We consider a first order in time approximation of the time derivatives and for the remaining terms in the system we use adequate implicit and semi-implicit approximations. Moreover, in order to reduce the computational cost of the scheme we have split the computation of the system into three different sub-steps. Apart from being more computationally efficient, another advantage of solving a splitting scheme instead of a fully coupled one is that this approach allows us to bypass dealing with some of the nonlinearities that relates unknowns that now are computed in different sub-steps. The proposed numerical scheme reads:

**Initialization:**

Let $\boldsymbol{u}^0 = \boldsymbol{u}|_{t=0}$, $\phi^0 = \phi|_{t=0}$, $\boldsymbol{d}^0 = \boldsymbol{d}|_{t=0}$ given in (3.13) and $\omega^0 \in W_h$ such that

$$\varepsilon\left(\omega^0,\bar{\omega}\right) - \varepsilon\left(\nabla\phi^0,\nabla\bar{\omega}\right) - \frac{1}{\varepsilon}\left(G(\phi^0),\bar{\omega}\right) = 0 \quad \forall\,\bar{\omega}\in W_h.$$

**Step** $n+1$:

Given $(\phi^n,\boldsymbol{d}^n,w^n)\in\Phi_h\times\boldsymbol{D}_h\times W_h$.

**Substep** 1: Find $(\boldsymbol{d}^{n+1},\boldsymbol{z}^{n+1})\in\boldsymbol{D}_h\times\boldsymbol{Z}_h$ such that, for each $(\bar{\boldsymbol{d}},\bar{\boldsymbol{z}})\in\boldsymbol{D}_h\times\boldsymbol{Z}_h$

$$\begin{cases} \left(\dfrac{\boldsymbol{d}^{n+1}-\boldsymbol{d}^n}{\Delta t},\bar{\boldsymbol{z}}\right) + \left((\boldsymbol{u}^\star\cdot\nabla)\boldsymbol{d}^n,\bar{\boldsymbol{z}}\right) \\ \qquad +\gamma_{nem}(\boldsymbol{z}^{n+1},\bar{\boldsymbol{z}}) = 0, \\ \lambda_{nem}\left(I(\phi^n)\nabla\boldsymbol{d}^{n+1},\nabla\bar{\boldsymbol{d}}\right) \\ +\lambda_{nem}\left(I(\phi^n)\boldsymbol{p}_{\Delta t}(\boldsymbol{d}^{n+1},\boldsymbol{d}^n),\bar{\boldsymbol{d}}\right) + \lambda_{anch} \\ \qquad\times\left(\Lambda_{\boldsymbol{d}}(\boldsymbol{d}^{n+1},\phi^n),\bar{\boldsymbol{d}}\right) - (\boldsymbol{z}^{n+1},\bar{\boldsymbol{d}}) = 0, \end{cases} \tag{3.18}$$

where

$$\boldsymbol{u}^\star := \boldsymbol{u}^n + 2\,\Delta t\,(\nabla\boldsymbol{d}^n)^t\boldsymbol{z}^{n+1},$$

$\Lambda_{\boldsymbol{d}}(\boldsymbol{d}^{n+1},\phi^n)$ and $\boldsymbol{p}_{\Delta t}(\boldsymbol{d}^{n+1},\boldsymbol{d}^n)$ denote first order approximations of $\dfrac{\delta E_{anch}}{\delta\boldsymbol{d}}(\boldsymbol{d}(t_{n+1}),\phi(t_{n+1}))$ and $\boldsymbol{p}(\boldsymbol{d}(t_{n+1}))$, respectively. In fact,

$$\Lambda_{\boldsymbol{d}}(\boldsymbol{d},\phi) := \frac{\delta E_{anch}}{\delta\boldsymbol{d}}(\boldsymbol{d},\phi) = \delta_1|\nabla\phi|^2\,\boldsymbol{d} + \delta_2\,(\boldsymbol{d}\cdot\nabla\phi)\,\nabla\phi,$$

with $(\delta_1,\delta_2)$ chosen as in (2.6).

**Substep** 2: Find $(\phi^{n+1},\mu^{n+1},\omega^{n+1})\in\Phi_h\times M_h\times W_h$ such that for any $(\bar{\phi},\bar{\mu},\bar{\omega})\in\Phi_h\times M_h\times W_h$:

$$\begin{cases} \left(\dfrac{\phi^{n+1}-\phi^n}{\Delta t},\bar{\mu}\right) - (\phi^n\boldsymbol{u}^{\star\star},\nabla\bar{\mu}) \\ \qquad +\gamma_{ben}(\nabla\mu^{n+1},\nabla\bar{\mu}) = 0, \\ \lambda_{bp}\varepsilon(\nabla\omega^{n+1},\nabla\bar{\phi}) + \dfrac{\lambda_{bp}}{\varepsilon}\left(G^{\Delta t}_{sec}(\phi^{n+1},\phi^n)\omega^{n+1},\bar{\phi}\right) \\ \qquad +\dfrac{\lambda_{bp}}{\eta}\left(\dfrac{B(\phi^{n+1})+B(\phi^n)}{2}-\beta\right) \\ \left(\varepsilon(\nabla\phi^{n+\frac{1}{2}},\nabla\bar{\phi}) + \frac{1}{\varepsilon}(F^{\Delta t}_{sec}(\phi^{n+1},\phi^n),\bar{\phi})\right) \\ \qquad +\lambda_{anch}\left(\Lambda_\phi(\boldsymbol{d}^{n+1},\phi^{n+1}),\nabla\bar{\phi}\right) \\ \qquad +\lambda_{nem}\left(i_{\Delta t}(\phi^{n+1},\phi^n)\left[\dfrac{1}{2}|\nabla\boldsymbol{d}^{n+1}|^2\right.\right. \\ \qquad \left.\left.+P(\boldsymbol{d}^{n+1})\right],\bar{\phi}\right) - (\mu^{n+1},\bar{\phi}) = 0, \\ \varepsilon\left(\omega^{n+1},\bar{\omega}\right) - \varepsilon\left(\nabla\phi^{n+1},\nabla\bar{\omega}\right) - \dfrac{1}{\varepsilon}\left(G(\phi^{n+1}),\bar{\omega}\right) = 0, \end{cases} \tag{3.19}$$

where

$$\boldsymbol{u}^{\star\star} := \boldsymbol{u}^n - 2\,\Delta t\,\phi^n\nabla\mu^{n+1},$$

$i_{\Delta t}(\phi^{n+1},\phi^n)$ and $-\nabla\cdot\Lambda_\phi(\boldsymbol{d}^{n+1},\phi^{n+1})$ represent first order approximations of $i(\phi(t_{n+1}))$ and $\dfrac{\delta E_{anch}}{\delta\phi}(\boldsymbol{d}(t_{n+1}),\phi(t_{n+1}))$, respectively. In fact,

$$\Lambda_\phi(\boldsymbol{d},\phi) := \delta_1\,|\boldsymbol{d}|^2\,\nabla\phi + \delta_2\,(\boldsymbol{d}\cdot\nabla\phi)\,\boldsymbol{d},$$

with the values of $(\delta_1,\delta_2)$ defined in (2.6). Moreover, $F^{\Delta t}_{sec}(\phi^{n+1},\phi^n)$ and $G^{\Delta t}_{sec}(\phi^{n+1},\phi^n)$ denote the nonlinear *secant type* approximations (see [51–53] and the references therein for different ways of handling these type of potentials):

$$\begin{aligned} F^{\Delta t}_{sec}(\phi^{n+1},\phi^n) &:= \frac{F(\phi^{n+1})-F(\phi^n)}{\phi^{n+1}-\phi^n} \\ &= \frac{1}{4}(\phi^{n+1}+\phi^n)((\phi^{n+1})^2+(\phi^n)^2-2) \end{aligned} \tag{3.20}$$

and

$$\begin{aligned} G^{\Delta t}_{sec}(\phi^{n+1},\phi^n) &:= \frac{G(\phi^{n+1})-G(\phi^n)}{\phi^{n+1}-\phi^n} = (\phi^{n+1}-\phi^n)^2 \\ &+ 3\left(\phi^{n+1}\phi^n - 1 - \varepsilon k(\boldsymbol{x})(\phi^{n+1}+\phi^n)\right). \end{aligned} \tag{3.21}$$

**Substep** 3 : Find $(\boldsymbol{u}^{n+1},p^{n+1})\in\boldsymbol{U}_h\times P_h$ such that for any $(\bar{\boldsymbol{u}},\bar{p})\in\boldsymbol{U}_h\times P_h$:

$$\begin{cases} \dfrac{1}{\Delta t}\left(\boldsymbol{u}^{n+1}-\widehat{\boldsymbol{u}},\bar{\boldsymbol{u}}\right) + c(\boldsymbol{u}^n,\boldsymbol{u}^{n+1},\bar{\boldsymbol{u}}) \\ +(2\nu(\phi^{n+1})\boldsymbol{D}\boldsymbol{u}^{n+1},\boldsymbol{D}\bar{\boldsymbol{u}}) - (p^{n+1},\nabla\cdot\bar{\boldsymbol{u}}) = 0, \\ (\nabla\cdot\boldsymbol{u}^{n+1},\bar{p}) = 0, \end{cases} \tag{3.22}$$

where

$$\widehat{\boldsymbol{u}} := \frac{\boldsymbol{u}^\star+\boldsymbol{u}^{\star\star}}{2} = \boldsymbol{u}^n + \Delta t\left((\nabla\boldsymbol{d}^n)^t\boldsymbol{z}^{n+1} - \phi^n\nabla\mu^{n+1}\right), \tag{3.23}$$

and $c(\cdot,\cdot,\cdot)$ is the trilinear antisymmetric form defined in (3.15).

### 3.3. Mass conservation

**Lemma 3.2.** *Scheme (3.19) satisfies the conservation of mass, that is,*

$$\int_\Omega \phi^{n+1} = \int_\Omega \phi^n = \ldots = \int_\Omega \phi^0.$$

**Proof.** Testing $(3.19)_1$ by $\bar\mu = 1$. ■

### 3.4. Energy stability

**Lemma 3.3.** *Scheme (3.18)–(3.23) satisfies the following discrete energy law (which is a discrete version of the energy law (2.12)),*

$$\begin{aligned}
&\delta_t \widetilde{E}_{tot}\left(\boldsymbol{u}^{n+1}, \phi^{n+1}, \boldsymbol{d}^{n+1}, \omega^{n+1}\right) + \left\| \sqrt{2\nu(\phi^{n+1})}\boldsymbol{D}\boldsymbol{u}^{n+1}\right\|_{L^2}^2 \\
&+\gamma_{ben}\|\nabla\mu^{n+1}\|_{L^2}^2 + \gamma_{nem}\|\boldsymbol{z}^{n+1}\|_{L^2}^2 \\
&+ND_{\boldsymbol{u}}^{n+1} + ND_{\omega}^{n+1} + ND_{elast}^{n+1} + ND_{penal}^{n+1} + ND_{interp}^{n+1} + ND_{anch}^{n+1} = 0\,,
\end{aligned} \tag{3.24}$$

*where the following numerical dissipation terms appear:*

$$\begin{cases}
ND_{\boldsymbol{u}}^{n+1} = \dfrac{1}{4\Delta t}\left(2\|\boldsymbol{u}^{n+1} - \widehat{\boldsymbol{u}}\|_{L^2}^2 + \|\widehat{\boldsymbol{u}} - \boldsymbol{u}^\star\|_{L^2}^2 + \|\widehat{\boldsymbol{u}} - \boldsymbol{u}^{\star\star}\|_{L^2}^2\right. \\
\qquad \left. +\|\boldsymbol{u}^\star - \boldsymbol{u}^n\|_{L^2}^2 + \|\boldsymbol{u}^{\star\star} - \boldsymbol{u}^n\|_{L^2}^2\right)\,, \\
ND_{\omega}^{n+1} = \lambda_{bp}\dfrac{\varepsilon\,\Delta t}{2}\|\delta_t\omega^{n+1}\|_{L^2}^2\,, \\
ND_{elast}^{n+1} = \lambda_{nem}\dfrac{\Delta t}{2}\displaystyle\int_\Omega I(\phi^n)\left|\delta_t\nabla\boldsymbol{d}^{n+1}\right|^2 d\boldsymbol{x}\,, \\
ND_{penal}^{n+1} = \lambda_{nem}\displaystyle\int_\Omega I(\phi^n)\left(\boldsymbol{p}_{\Delta t}(\boldsymbol{d}^{n+1}, \boldsymbol{d}^n)\right. \\
\qquad \left.\cdot\delta_t\boldsymbol{d}^{n+1} - \delta_t P(\boldsymbol{d}^{n+1})\right) d\boldsymbol{x}\,, \\
ND_{interp}^{n+1} = \lambda_{nem}\displaystyle\int_\Omega\left(\frac{|\nabla\boldsymbol{d}^{n+1}|^2}{2} + G(\boldsymbol{d}^{n+1})\right) \\
\qquad \times\left(i_{\Delta t}(\phi^{n+1}, \phi^n)\,\delta_t\phi^{n+1} - \delta_t I(\phi^{n+1})\right) d\boldsymbol{x}\,,
\end{cases}$$

*and*

$$\begin{aligned}
ND_{anch}^{n+1} = \lambda_{anch}\frac{\Delta t}{2}\int_\Omega &\left[\delta_1\left(|\delta_t\boldsymbol{d}^{n+1}|^2|\nabla\phi^n|^2 + |\boldsymbol{d}^{n+1}|^2|\delta_t\nabla\phi^{n+1}|^2\right)\right. \\
&+\delta_2\left(|\delta_t\boldsymbol{d}^{n+1}\cdot\nabla\phi^n|^2\right. \\
&\left.\left.+|\boldsymbol{d}^{n+1}\cdot\nabla\delta_t\phi^{n+1}|^2\right)\right] d\boldsymbol{x}\,,
\end{aligned}$$

*with the values of $(\delta_1, \delta_2)$ depending on the type of anchoring defined in (2.6).*

**Proof.** For the sake of simplicity we will only show the case of homeotropic anchoring (the parallel anchoring case can be studied using the same arguments while the no anchoring case is just a trivial generalization).

Taking $(\bar{\boldsymbol{z}}, \bar{\boldsymbol{d}}) = (\boldsymbol{z}^{n+1}, \delta_t\boldsymbol{d}^{n+1})$ in (3.18), we obtain:

$$\begin{aligned}
&\gamma_{nem}\|\boldsymbol{z}^{n+1}\|_{L^2}^2 + ND_{elast}^{n+1} + ND_{penal}^{n+1} + \left((\boldsymbol{u}^\star\cdot\nabla)\boldsymbol{d}^n, \boldsymbol{z}^{n+1}\right) \\
&+\lambda_{nem}\int_\Omega I(\phi^n)\,\delta_t\left(\frac{|\nabla\boldsymbol{d}^{n+1}|^2}{2} + P(\boldsymbol{d}^{n+1})\right) d\boldsymbol{x} \\
&+\frac{\lambda_{anch}}{2\Delta t}\,\delta_1\int_\Omega\left[|\nabla\phi^n|^2|\boldsymbol{d}^{n+1}|^2 - |\nabla\phi^n|^2|\boldsymbol{d}^n|^2\right] d\boldsymbol{x} \\
&+\frac{\lambda_{anch}}{2\Delta t}\,\delta_2\int_\Omega\left[|\boldsymbol{d}^{n+1}\cdot\nabla\phi^n|^2 - |\boldsymbol{d}^n\cdot\nabla\phi^n|^2\right] d\boldsymbol{x} \\
&+\frac{\lambda_{anch}}{2}\Delta t\int_\Omega\left[\delta_1|\delta_t\boldsymbol{d}^{n+1}|^2|\nabla\phi^{n+1}|^2 + \delta_2|\delta_t\boldsymbol{d}^{n+1}\cdot\nabla\phi^n|^2\right] d\boldsymbol{x} = 0\,.
\end{aligned} \tag{3.25}$$

On the other hand, taking $(\bar\mu, \bar\phi) = (\mu^{n+1}, \delta_t\phi^{n+1})$ in $(3.19)_{1,2}$, adding the resulting expressions and taking into account the definition of $F_{sec}^{\Delta t}(\phi^{n+1}, \phi^n)$ and $G_{sec}^{\Delta t}(\phi^{n+1}, \phi^n)$ given in (3.20) and (3.21), that is,

$$\begin{aligned}
&\frac{1}{\varepsilon}\left(G_{sec}^{\Delta t}(\phi^{n+1}, \phi^n)\omega^{n+1}, \delta_t\phi^{n+1}\right) = \frac{1}{\varepsilon\,\Delta t}\left(G(\phi^{n+1}) - G(\phi^n), \omega^{n+1}\right), \\
&\left(\varepsilon(\nabla\phi^{n+\frac12}, \nabla\delta_t\phi^{n+1}) + \frac{1}{\varepsilon}(F_{sec}^{\Delta t}(\phi^{n+1}, \phi^n), \delta_t\phi^{n+1})\right) \\
&= B(\phi^{n+1}) - B(\phi^n),
\end{aligned}$$

we obtain

$$\begin{aligned}
&\gamma_{ben}\|\nabla\mu^{n+1}\|_{L^2}^2 + \varepsilon(\nabla\omega^{n+1}, \nabla\delta_t\phi^{n+1}) - (\phi^n\boldsymbol{u}^{\star\star}, \nabla\mu^{n+1}) \\
&+\frac{1}{\varepsilon\,\Delta t}\left(G(\phi^{n+1}) - G(\phi^n), \omega^{n+1}\right) + \frac{1}{2\eta}\delta_t\left(B(\phi^{n+1}) - \beta\right)^2 + ND_{interp}^{n+1} \\
&+\lambda_{nem}\int_\Omega\left(\frac{|\nabla\boldsymbol{d}^{n+1}|^2}{2} + G(\boldsymbol{d}^{n+1})\right)\delta_t I(\phi^{n+1})d\boldsymbol{x} \\
&+\frac{\lambda_{anch}}{2\Delta t}\,\delta_1\int_\Omega\left[|\nabla\phi^{n+1}|^2|\boldsymbol{d}^{n+1}|^2 - |\nabla\phi^n|^2|\boldsymbol{d}^{n+1}|^2\right] d\boldsymbol{x} \\
&+\frac{\lambda_{anch}}{2\Delta t}\,\delta_2\int_\Omega\left[|\boldsymbol{d}^{n+1}\cdot\nabla\phi^{n+1}|^2 - |\boldsymbol{d}^{n+1}\cdot\nabla\phi^n|^2\right] d\boldsymbol{x} \\
&+\frac{\lambda_{anch}}{2}\Delta t\int_\Omega\left[\delta_1|\boldsymbol{d}^{n+1}|^2|\nabla\delta_t\phi^{n+1}|^2 + \delta_2|\boldsymbol{d}^{n+1}\cdot\nabla\delta_t\phi^{n+1}|^2\right] d\boldsymbol{x} \\
&= 0\,.
\end{aligned} \tag{3.26}$$

Subtracting $(3.19)_{3,\text{split-23}}$ for previous time step, and dividing by $\Delta t$, we obtain

$$\varepsilon(\delta_t\omega^{n+1}, \bar\omega) - \varepsilon\left(\nabla\delta_t\phi^{n+1}, \nabla\bar\omega\right) - \frac{1}{\varepsilon\,\Delta t}\left(G(\phi^{n+1}) - G(\phi^n), \bar\omega\right) = 0.$$

Then taking $\bar\omega = \omega^{n+1}$, we obtain

$$\begin{aligned}
&\frac{\varepsilon}{2}\delta_t\|\omega^{n+1}\|_{L^2}^2 + ND_{\omega}^{n+1} - \varepsilon\left(\nabla\delta_t\phi^{n+1}, \nabla\omega^{n+1}\right) \\
&\quad - \frac{1}{\varepsilon\,\Delta t}\left(G(\phi^{n+1}) - G(\phi^n), \omega^{n+1}\right) = 0\,.
\end{aligned} \tag{3.27}$$

Adding relations (3.26) and (3.27), the terms $\varepsilon\left(\nabla\delta_t\phi^{n+1}, \nabla\omega^{n+1}\right)$ and $\frac{1}{\varepsilon\,\Delta t}\left(G(\phi^{n+1}) - G(\phi^n), \omega^{n+1}\right)$ cancel, hence we derive :

$$\begin{aligned}
&\delta_t\widetilde{E}_{bp}(\omega^{n+1}, \phi^{n+1}) + \gamma_{ben}\|\nabla\mu^{n+1}\|_{L^2}^2 + ND_{\omega}^{n+1} + ND_{interp}^{n+1} \\
&+\lambda_{nem}\int_\Omega\left(\frac{|\nabla\boldsymbol{d}^{n+1}|^2}{2} + G(\boldsymbol{d}^{n+1})\right)\delta_t I(\phi^{n+1})d\boldsymbol{x} \\
&+\frac{\lambda_{anch}}{2\Delta t}\,\delta_1\int_\Omega\left[|\nabla\phi^{n+1}|^2|\boldsymbol{d}^{n+1}|^2 - |\nabla\phi^n|^2|\boldsymbol{d}^{n+1}|^2\right] d\boldsymbol{x} \\
&+\frac{\lambda_{anch}}{2\Delta t}\,\delta_2\int_\Omega\left[|\boldsymbol{d}^{n+1}\cdot\nabla\phi^{n+1}|^2 - |\boldsymbol{d}^{n+1}\cdot\nabla\phi^n|^2\right] d\boldsymbol{x} \\
&+\frac{\lambda_{anch}}{2}\Delta t\int_\Omega\left[\delta_1|\boldsymbol{d}^{n+1}|^2|\nabla\delta_t\phi^{n+1}|^2 + \delta_2|\boldsymbol{d}^{n+1}\cdot\nabla\delta_t\phi^{n+1}|^2\right] d\boldsymbol{x} \\
&= 0\,.
\end{aligned} \tag{3.28}$$

Following the same argument presented in Proof of Theorem 32 in [41] we obtain

$$\begin{aligned}
&\frac{1}{\Delta t}\left(\frac12\|\boldsymbol{u}^{n+1}\|_{L^2}^2 - \frac12\|\boldsymbol{u}^n\|_{L^2}^2\right) \\
&\quad +\|\sqrt{2\nu(\phi^{n+1})}\nabla\boldsymbol{u}^{n+1}\|_{L^2}^2 + ND_{\boldsymbol{u}}^{n+1} \\
&+(\phi^n\boldsymbol{u}^{\star\star}, \nabla\mu^{n+1}) - \left((\boldsymbol{u}^\star\cdot\nabla)\boldsymbol{d}^n, \boldsymbol{z}^{n+1}\right) \quad = \quad 0\,.
\end{aligned} \tag{3.29}$$

Adding expressions (3.25), (3.28) and (3.29), we arrive at the desired equality (3.24). ■

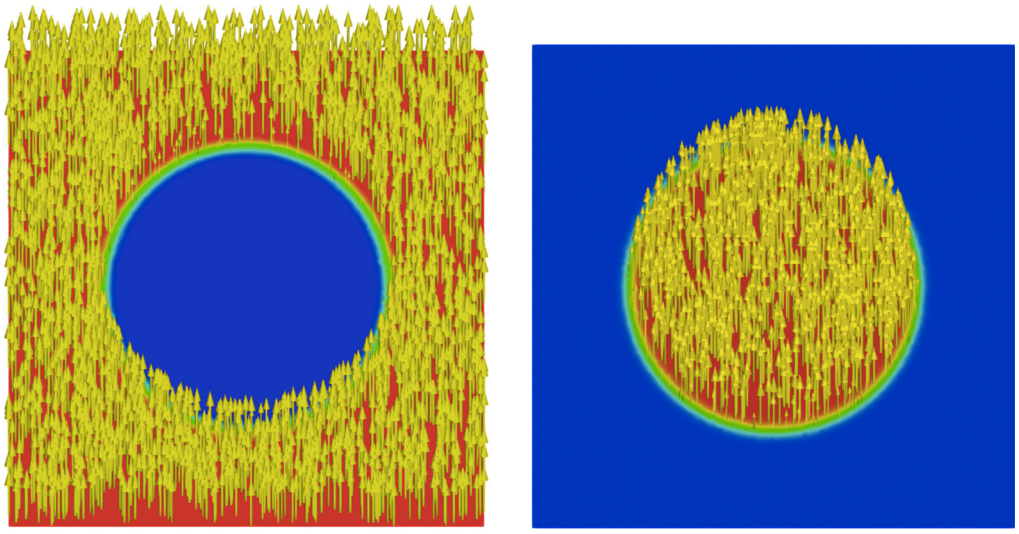

**Fig. 1.** Initial conditions of $\phi$ (vesicle) and $\boldsymbol{d}$ (nematic liquid crystal orientation) considered in Example I for studying the contribution of the anchoring effects to the dynamics of the system.

**Remark 3.4.** From (3.24) it is clear that scheme (3.18)–(3.19)–(3.22) is unconditional energy-stable with respect to the modified energy $\widetilde{E}_{tot}(\boldsymbol{u}, \phi, \boldsymbol{d}, \omega)$, that is

$$\widetilde{E}_{tot}(\boldsymbol{u}^{n+1}, \phi^{n+1}, \boldsymbol{d}^{n+1}, \omega^{n+1}) \leq \widetilde{E}_{tot}(\boldsymbol{u}^{n}, \phi^{n}, \boldsymbol{d}^{n}, \omega^{n}) \quad \forall\, n,$$

if we consider approximations of the nonlinear terms $\boldsymbol{p}_{\Delta t}(\boldsymbol{d}^{n+1}, \boldsymbol{d}^n)$ and $i_{\Delta t}(\phi^{n+1}, \phi^n)$ such that

$$ND^{n+1}_{penal} \geq 0 \quad \text{and} \quad ND^{n+1}_{interp} \geq 0\,. \tag{3.30}$$

There are several ways of achieving this goal, but we will consider the approximations introduced in [41] (where it is shown that these approximations satisfy (3.30))

$$\begin{aligned} \boldsymbol{p}_{\Delta t}(\boldsymbol{d}^{n+1}, \boldsymbol{d}^n) &= \widetilde{\boldsymbol{p}}(\boldsymbol{d}^n) + \frac{1}{2}\,\|\widetilde{\boldsymbol{p}}'(\boldsymbol{d})\|_\infty\,(\boldsymbol{d}^{n+1} - \boldsymbol{d}^n)\,, \\ i_{\Delta t}(c^{n+1}, c^n) &= i(c^n) + \frac{5\sqrt{3}}{12}\,(c^{n+1} - c^n)\,, \end{aligned} \tag{3.31}$$

with

$$\widetilde{\boldsymbol{p}}(\boldsymbol{d}) = \begin{cases} \dfrac{2}{\eta_{\boldsymbol{d}}^2}\,(|\boldsymbol{d}| - 1)\,\dfrac{\boldsymbol{d}}{|\boldsymbol{d}|} & \text{if } |\boldsymbol{d}| \geq 1\,, \\ \dfrac{1}{\eta_{\boldsymbol{d}}^2}(|\boldsymbol{d}|^2 - 1)\,\boldsymbol{d} & \text{if } |\boldsymbol{d}| \leq 1\,. \end{cases}$$

**Lemma 3.5.** *Scheme (3.18)–(3.19)–(3.22) considering the approximations of $\boldsymbol{p}_{\Delta t}(\boldsymbol{d}^{n+1}, \boldsymbol{d}^n)$ and $i_{\Delta t}(\phi^{n+1}, \phi^n)$ presented in (3.31) is unconditionally energy-stable with respect to $\widetilde{E}_{tot}(\boldsymbol{u}, \phi, \boldsymbol{d}, \omega)$.*

## 4. Simulations

The aim of this section is to present the results of several numerical simulations to display the type of dynamics exhibited by the proposed model as well as to illustrate the efficiency and accuracy of the numerical scheme derived in the paper. In particular, we have considered the scheme presented in (3.18)–(3.19)–(3.22) with the boundary conditions presented in (2.11) unless mentioned otherwise, using the approximations of $\boldsymbol{p}_{\Delta t}(\boldsymbol{d}^{n+1}, \boldsymbol{d}^n)$ and $i_{\Delta t}(\phi^{n+1}, \phi^n)$ presented in (3.31) and for the sake of simplicity we only consider the case with no spontaneous curvature ($k(\boldsymbol{x}) = 0$).

All the simulations have been carried out in 2*D* domains using *FreeFem++* software [54] and the discrete spaces considered are $(\mathbb{P}_2 \times \mathbb{P}_1)$ for the pair $(\boldsymbol{U}_h, P_h)$ (Taylor–Hood element) and $\mathbb{P}_1$ for $\boldsymbol{D}_h$, $\boldsymbol{Z}_h$, $\Phi_h$, $M_h$ and $W_h$. In the first example we demonstrate how the anchoring effects play an important role in the shapes of the vesicles. Then, in the second example we perform a numerical test to prove the accuracy of the proposed scheme. After that, we study how in the case of vesicles filled with nematic liquid crystal, the internal configuration of the liquid crystal also plays an important role on the achievable shapes of the vesicles. In the rest of the examples we focus on the interaction of the vesicles with the flow, showing that our approach is able to capture interesting features such as rotation of the vesicles in rotating fluids, deformation through constrictions and axisymmetric shapes of the bullet-like shape (with a convex rear end) and the parachute-like shape (with a concave rear end) when the vesicles are transported by Poiseuille flows.

**Table 1**
Parameters considered in Example I.

| $h$ | $\Delta t$ | $\lambda_{bp}$ | $\lambda_{nem}$ | $\lambda_{anch}$ | $\gamma_{nem}$ | $\gamma_{ben}$ | $\varepsilon$ | $\eta_{\boldsymbol{d}}$ | $\eta$ | $\nu_{Nw}$ | $\nu_{Lc}$ |
|---|---|---|---|---|---|---|---|---|---|---|---|
| 1/100 | $10^{-5}$ | 0.01 | 100.1 | 100.1 | 0.5 | 0.01 | 0.01 | 0.075 | $10^{-5}$ | 1.0 | 1.0 |

### 4.1. Example I. Anchoring effects

In this first example we study the influence of the anchoring effects in the dynamics of the system. We consider initially circular configurations of the vesicles and we study the evolution of the system depending on the different anchoring cases considered. The domain considered for this example is a square ($\Omega = [0, 1]^2$), the imposed surface area of the vesicle corresponds with the initial one (that is, $\beta = B(\phi^0)$) and the discrete and physical parameters are presented in Table 1. We have considered two different types of simulations, ones where the vesicles are filled with newtonian fluid and immersed in a nematic liquid crystal and the other way around, that is, ones where the vesicles are filled with nematic liquid crystal and immersed in a newtonian fluid. The initial configurations considered for the simulations are presented in Fig. 1. The equilibrium configurations obtained for the three types of anchoring effects in each case are presented in Figs. 2 and 3, where it is observed that the considered choice of parameters produces that the anchoring effects are strong enough to deform the vesicle to accommodate their influence. The evolution of $\widetilde{E}_{tot}$ (total energy), $E_{kin}$ (kinetic energy), $\int_\Omega \phi$

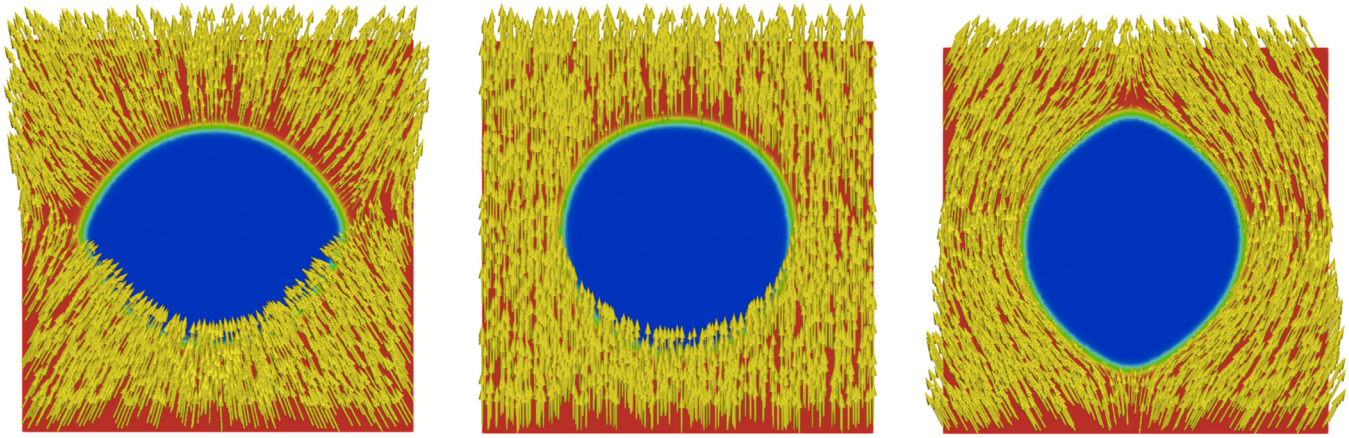

**Fig. 2.** Equilibrium configurations of $\phi$ (vesicle) and $\boldsymbol{d}$ (nematic liquid crystal orientation) using as initial condition the configuration in the left side of Fig. 1. Left: Homeotropic Anchoring ($(\delta_1, \delta_2) = (1, -1)$). Center: No Anchoring ($(\delta_1, \delta_2) = (0, 0)$). Right: Parallel Anchoring ($(\delta_1, \delta_2) = (0, 1)$).

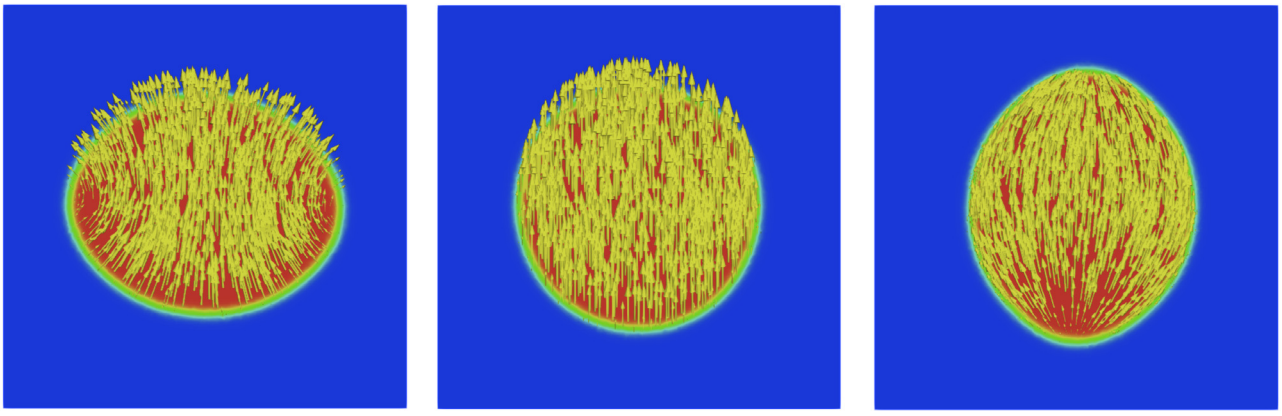

**Fig. 3.** Equilibrium configurations of $\phi$ (vesicle) and $\boldsymbol{d}$ (nematic liquid crystal orientation) using as initial condition the configuration in the right side of Fig. 1. Left: Homeotropic Anchoring ($(\delta_1, \delta_2) = (1, -1)$). Center: No Anchoring ($(\delta_1, \delta_2) = (0, 0)$). Right: Parallel Anchoring ($(\delta_1, \delta_2) = (0, 1)$).

(volume) and $B(\phi)$ (surface) are presented in Figs. 4 and 5, respectively. These results show that the deformation of the systems to accommodate the anchoring effects produce movement of the fluid part, movement that results in an increasing kinetic energy but maintaining the expected decreasing property of the total energy (this is expected in the original problem due to (2.12) and numerically due to (3.24)). Moreover, the surface of the resulting vesicles are close to the original ones although they are not exactly conserved. This is due to the fact that this conservation of surface is imposed through an energy that forms part of the total energy. Minimizing the total energy (that represents the combination of very different effects) does not imply that the system will arrive to a configuration where all the sub-energies achieve their possible minimums, because there is a combination of interests (for instance perfectly achieved conservation of surface could lead to configurations that are not satisfactory to the anchoring energy). Finally we can observe that the volume of the systems remain constant as expected (check Lemma 3.2).

### 4.2. Example II. Accuracy study

In this second example a numerical error estimate in time is estimated. The domain considered for this example is a square ($\Omega = [0, 1]^2$), the imposed surface area of the vesicle corresponds with the initial one (that is, $\beta = B(\phi^0)$), the initial configuration is the one presented in the left side of Fig. 1, the physical parameters for this test are the ones used in Example I, that is the ones detailed in Table 1, we consider homeotropic anchoring ($(\delta_1, \delta_2) = (1, -1)$) and the final time considered is $T = 10^{-4}$. The parameters are chosen in such a way that the dynamic is not at equilibrium yet. We compute the EOC (Experimental Order of Convergence) using as reference (or exact) solution the one obtained by solving the system using scheme discretization parameters $h = 1/200$ and $\Delta t = 10^{-8}$, configuration that is presented in Fig. 6.

We now introduce some additional notation. The individual errors using discrete norms and the convergence rate between two consecutive time steps of size $\Delta t$ and $\widetilde{\Delta t}$ are defined as

$$e_2(\theta) := \frac{\|\theta_{exact} - \theta_h\|_{L^2(\Omega)}}{\|\theta_{exact}\|_{L^2(\Omega)}}, \quad e_1(\theta) := \frac{\|\theta_{exact} - \theta_h\|_{H^1(\Omega)}}{\|\theta_{exact}\|_{H^1(\Omega)}} \quad \text{and}$$

$$r_i(\cdot) := \left[\log\left(\frac{e_i(\cdot)}{\tilde{e}_i(\cdot)}\right)\right] \Big/ \left[\log\left(\frac{\Delta t}{\widetilde{\Delta t}}\right)\right].$$

The convergence history for a sequence of time steps using $h = 1/200$ is presented in Table 2. We can observe that all the unknowns show a good performance from the order of convergence point of view, because all the unknowns seem to achieve order one (higher orders of convergence are not expected for splitting schemes like the one we are considering). On the other hand, some of the errors might seem high and this is related with a combination of several facts: (1) the system that we are approximating is highly nonlinear; (2) we are comparing the solutions in a challenging setting, where the system has not achieved an equilibrium yet.

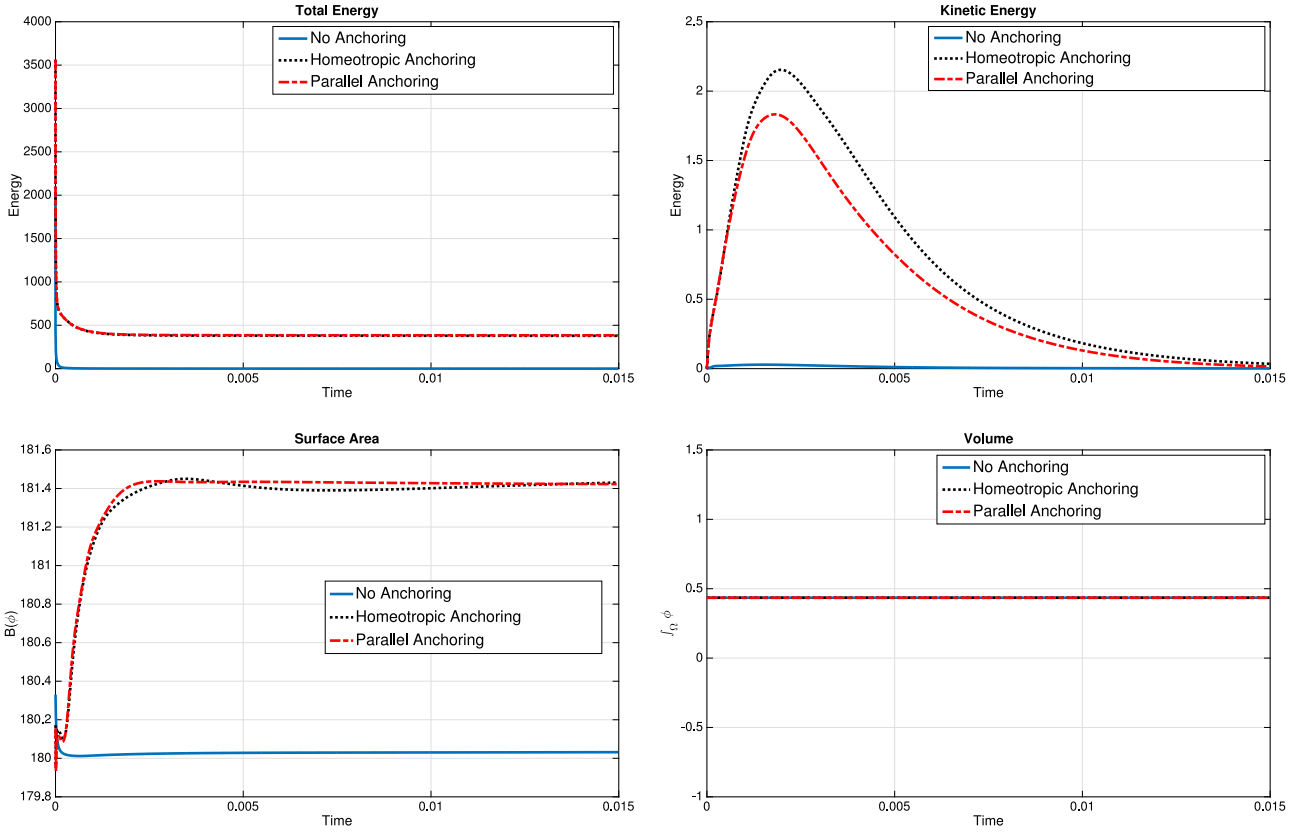


**Fig. 4.** Example I. Results considering as initial condition the configuration in the left side of Fig. 1. Top Left: Evolution of Total Energy. Top Right: Evolution of Kinetic Energy. Bottom Left: Evolution of $B(\phi)$. Bottom Right: Evolution of $\int_\Omega \phi$.

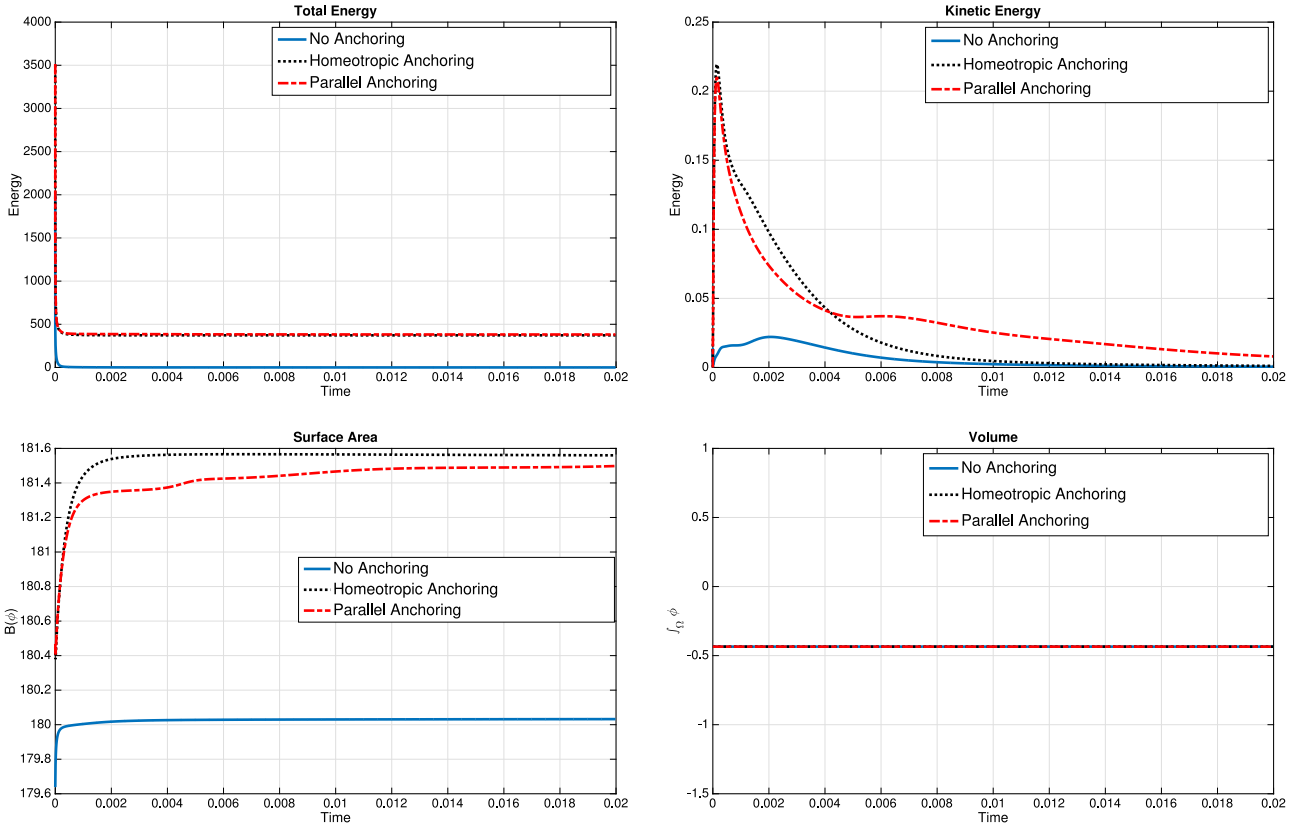


**Fig. 5.** Example I. Results considering as initial condition the configuration in the right side of Fig. 1. Top Left: Evolution of Total Energy. Top Right: Evolution of Kinetic Energy. Bottom Left: Evolution of $B(\phi)$. Bottom Right: Evolution of $\int_\Omega \phi$.

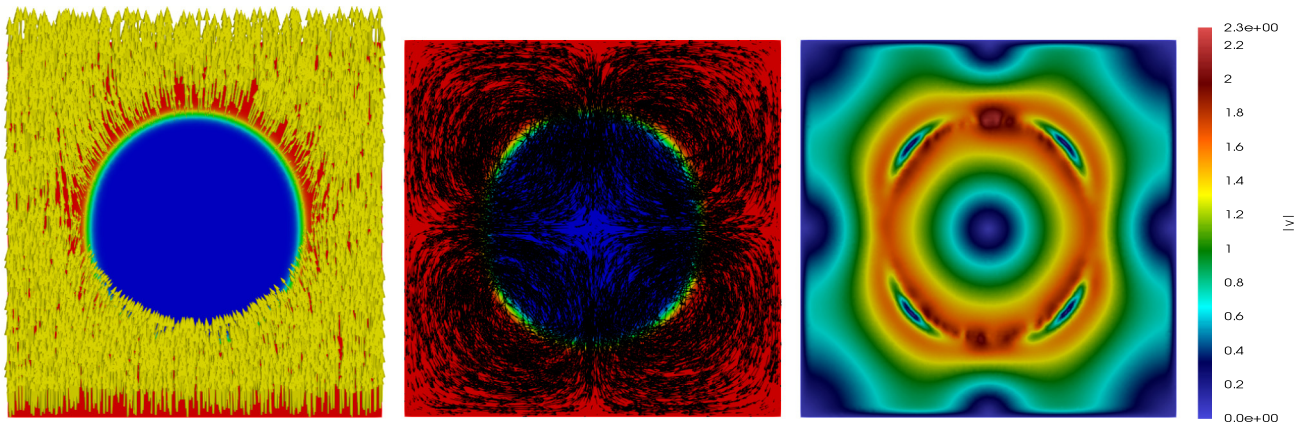


**Fig. 6.** Example II. Reference solution considered for computing the Experimental Order of Convergence of the scheme with $h = 1/200$ and $\Delta t = 10^{-8}$. Left: $\phi$ (vesicle) and $\boldsymbol{d}$ (nematic liquid crystal orientation), Center: $\phi$ (vesicle) and $\boldsymbol{u}$ (velocity), Right: $|\boldsymbol{u}|$ (velocity magnitude).

**Table 2**
Example II. Experimental absolute errors and order of convergences using the physical parameters detailed in Table 1 with $h = 1/200$ and reference solution computed using $h = 1/200$ and $\Delta t = 10^{-8}$.

| $\Delta t$ | $e_2(\boldsymbol{d})$ | $r_2(\boldsymbol{d})$ | $e_1(\boldsymbol{d})$ | $r_1(\boldsymbol{d})$ | $e_2(\boldsymbol{z})$ | $r_2(\boldsymbol{z})$ | $e_2(\phi)$ | $r_2(\phi)$ | $e_1(\phi)$ | $r_1(\phi)$ |
|---|---|---|---|---|---|---|---|---|---|---|
| $1 \times 10^{-5}$ | 0.0303 | – | 0.0549 | – | 0.2938 | – | 0.0300 | – | 0.0106 | – |
| $5 \times 10^{-6}$ | 0.0187 | 0.6975 | 0.0389 | 0.4978 | 0.1530 | 0.9413 | 0.0218 | 0.4600 | 0.0077 | 0.4573 |
| $2 \times 10^{-6}$ | 0.0097 | 0.7174 | 0.0221 | 0.6188 | 0.0696 | 0.8597 | 0.0125 | 0.6063 | 0.0044 | 0.6051 |
| $10^{-6}$ | 0.0056 | 0.7865 | 0.0132 | 0.7424 | 0.0384 | 0.8568 | 0.0075 | 0.7424 | 0.0026 | 0.7420 |
| $10^{-7}$ | 0.0006 | 0.9415 | 0.0016 | 0.9291 | 0.0042 | 0.9639 | 0.0009 | 0.9316 | 0.0003 | 0.9316 |

| $\Delta t$ | $e_2(\mu)$ | $r_2(\mu)$ | $e_1(\mu)$ | $r_1(\mu)$ | $e_2(\omega)$ | $r_2(\omega)$ | $e_1(\omega)$ | $r_1(\omega)$ |
|---|---|---|---|---|---|---|---|---|
| $1 \times 10^{-5}$ | 1.0352 | – | 0.0009 | – | 0.1197 | – | 0.0939 | – |
| $5 \times 10^{-6}$ | 0.3733 | 1.4713 | 0.00036 | 1.3290 | 0.0799 | 0.5826 | 0.0664 | 0.4987 |
| $2 \times 10^{-6}$ | 0.0770 | 1.7234 | 0.0001 | 1.3179 | 0.0445 | 0.6385 | 0.0383 | 0.6010 |
| $10^{-6}$ | 0.0200 | 1.9438 | 0.000048 | 1.1393 | 0.0265 | 0.7479 | 0.0231 | 0.7300 |
| $10^{-7}$ | 0.0031 | 0.8039 | 0.000005 | 0.9753 | 0.0031 | 0.9307 | 0.0027 | 0.9248 |

| $\Delta t$ | $e_2(\boldsymbol{u})$ | $r_2(\boldsymbol{u})$ | $e_1(\boldsymbol{u})$ | $r_1(\boldsymbol{u})$ | $e_2(p)$ | $r_2(p)$ |
|---|---|---|---|---|---|---|
| $1 \times 10^{-5}$ | 0.2856 | – | 0.0254 | – | 0.3995 | – |
| $5 \times 10^{-6}$ | 0.1921 | 0.5719 | 0.0187 | 0.4387 | 0.2002 | 0.9966 |
| $2 \times 10^{-6}$ | 0.1017 | 0.6938 | 0.0111 | 0.5750 | 0.0806 | 0.9932 |
| $10^{-6}$ | 0.0588 | 0.7908 | 0.0068 | 0.7122 | 0.0406 | 0.9900 |
| $10^{-7}$ | 0.0067 | 0.9404 | 0.0008 | 0.9169 | 0.0038 | 1.0278 |

### 4.3. Example III. Evolution of defects inside a circular vesicle

In this example we study the evolution of circular vesicles filled with nematic liquid crystal immersed in an isotropic fluid, where the initial configuration of the liquid crystal includes two defects, a hedgehog and an anti-hedgehog one. The domain considered for this example is a square ($\Omega = [0, 1]^2$), the imposed surface area of the vesicle corresponds with the initial one (that is, $\beta = B(\phi^0)$) and the discrete and physical parameters are the ones presented in Table 1 (the same values that were considered in Example I).

In Figs. 7–9 we present the dynamics for the different types of anchoring effects considered (homeotropic anchoring, no anchoring and parallel anchoring, respectively). In the three cases the systems are trying to eliminate the two defects to decrease the total energy of the system, producing movement on the fluid part of the system, and this movement contributes to push the defects closer to the interface, where they can be eliminated. Interestingly, in the homeotropic case not both defects can be eliminated, due to the fact that the initial configuration of $\boldsymbol{d}$ (nematic liquid crystal orientation) is close to be optimal from the anchoring effect point of view, and with this choice of parameters it seems energetically better for the system to maintain the defect in order not to increase the anchoring energy while trying to eliminate it. In fact, what the system does is to move the defect to the center, producing that the anchoring energy with this radial configuration is going to be very small. It is interesting to note that these equilibrium configurations are in accordance with the experimental and numerical results presented in [15]. The evolution of $\widetilde{E}_{tot}$ (total energy), $E_{kin}$ (kinetic energy), $\int_\Omega \phi$ (volume) and $B(\phi)$ (surface) are presented in Fig. 10. We observe that the total energy of the systems decrease in time, corroborating the results of Lemma 3.3. The volume of the system is exactly conserved (as expected) and the surface of the vesicles is not exactly conserved but it remains in a range of values close to the desired one (again, this is due to the fact that we are imposing the conservation of surface through the energy).

### 4.4. Example IV. Rotation of vesicles

This section is devoted to show that the presented numerical scheme is able to simulate vesicles rotating as a whole like rigid bodies, as it is known to happen in the tumbling regime [6]. For simplicity we have considered the case where no anchoring effects are imposed ($(\delta_1, \delta_2) = (0, 0)$). The domain considered for this example is a square ($\Omega = [0, 1]^2$), the imposed surface area of the vesicle corresponds with the initial one (that is, $\beta = B(\phi^0)$) and the discrete and physical parameters are the ones presented in Table 3.

The initial conditions are a elliptical configuration of the vesicle, $\boldsymbol{d}^0 = (0, 1)$ and the initial and boundary conditions for the

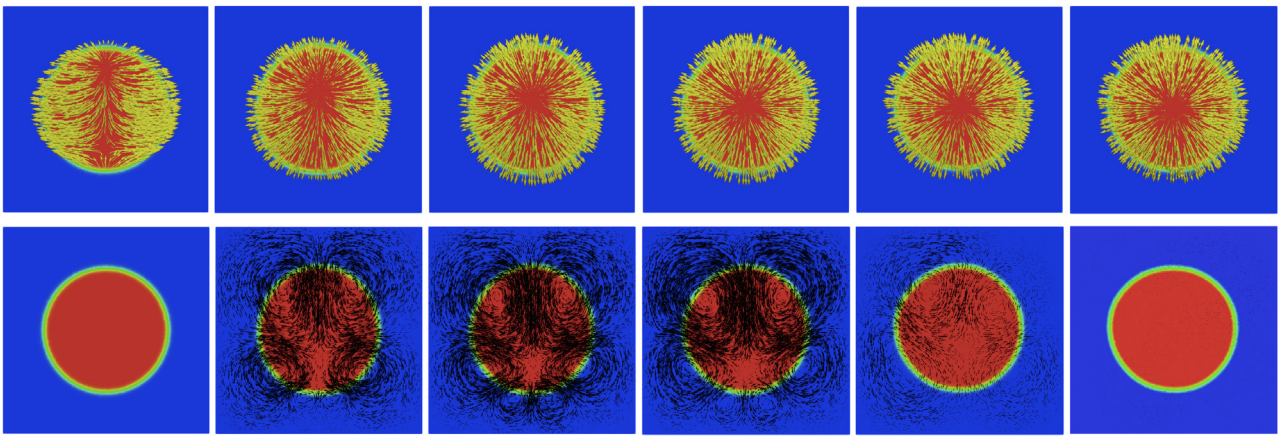

**Fig. 7.** Example III. Dynamics of a vesicle filled with nematic liquid crystal immersed in an isotropic fluid with Homeotropic Anchoring ($(\delta_1, \delta_2) = (1, -1)$) at times $t = 0, 0.0005, 0.001, 0.0025, 0.01, 0.03$. Top: $\phi$ (vesicle) and $\boldsymbol{d}$ (nematic liquid crystal orientation). Bottom: $\phi$ (vesicle) and $\boldsymbol{u}$ (fluid).

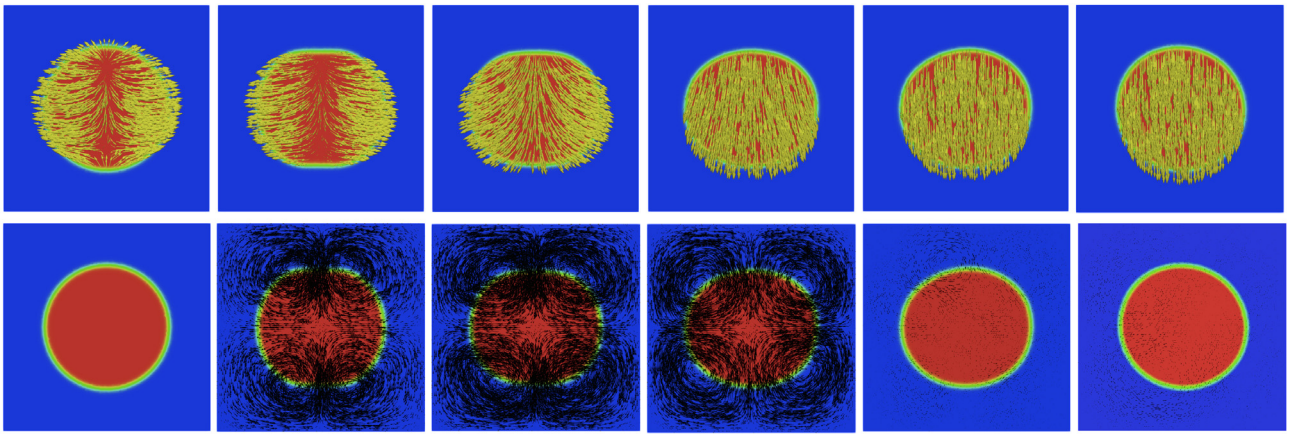

**Fig. 8.** Example III. Dynamics of a vesicle filled with nematic liquid crystal immersed in an isotropic fluid with No Anchoring ($(\delta_1, \delta_2) = (0, 0)$) at times $t = 0, 0.0005, 0.001, 0.0025, 0.01, 0.03$. Top: $\phi$ (vesicle) and $\boldsymbol{d}$ (nematic liquid crystal orientation). Bottom: $\phi$ (vesicle) and $\boldsymbol{u}$ (fluid).

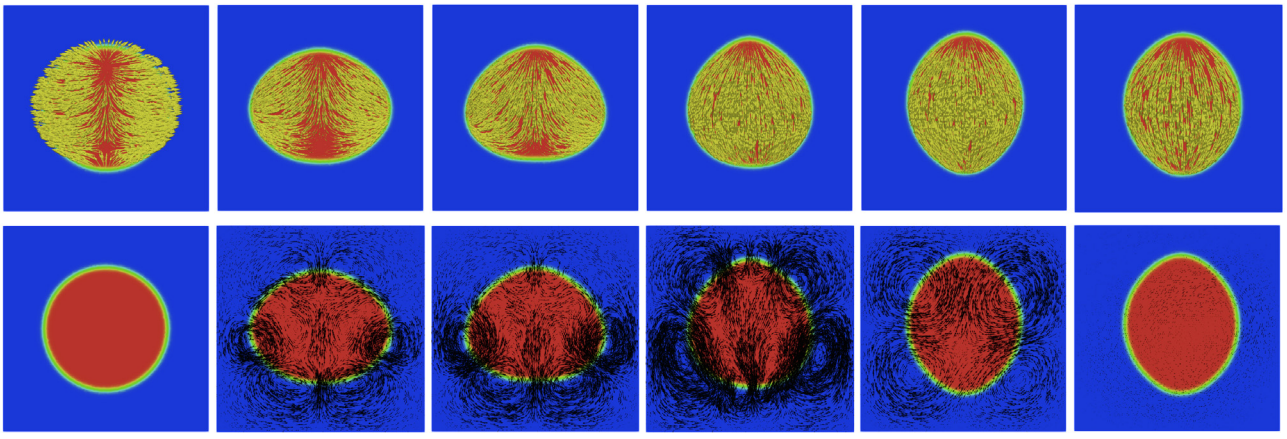

**Fig. 9.** Example III. Dynamics of a vesicle filled with nematic liquid crystal immersed in an isotropic fluid with Parallel Anchoring ($(\delta_1, \delta_2) = (0, 1)$) at times $t = 0, 0.0005, 0.001, 0.0025, 0.01, 0.03$. Top: $\phi$ (vesicle) and $\boldsymbol{d}$ (nematic liquid crystal orientation). Bottom: $\phi$ (vesicle) and $\boldsymbol{u}$ (fluid).

fluid velocity are given by

$$\boldsymbol{u}^0 = \boldsymbol{u}|_{\partial\Omega_{top}} = \big( 2000\pi \cos(\pi y)\sin(\pi x)^2, \\ -4000\pi \cos(\pi x)\sin(\pi x)\sin(\pi y) \big) .$$

The dynamics of the system are presented in Fig. 11 and the evolution of $B(\phi)$ and the volume $\int_\Omega \phi$ in Fig. 12. It can be observed that with this choice of parameters the vesicle does not

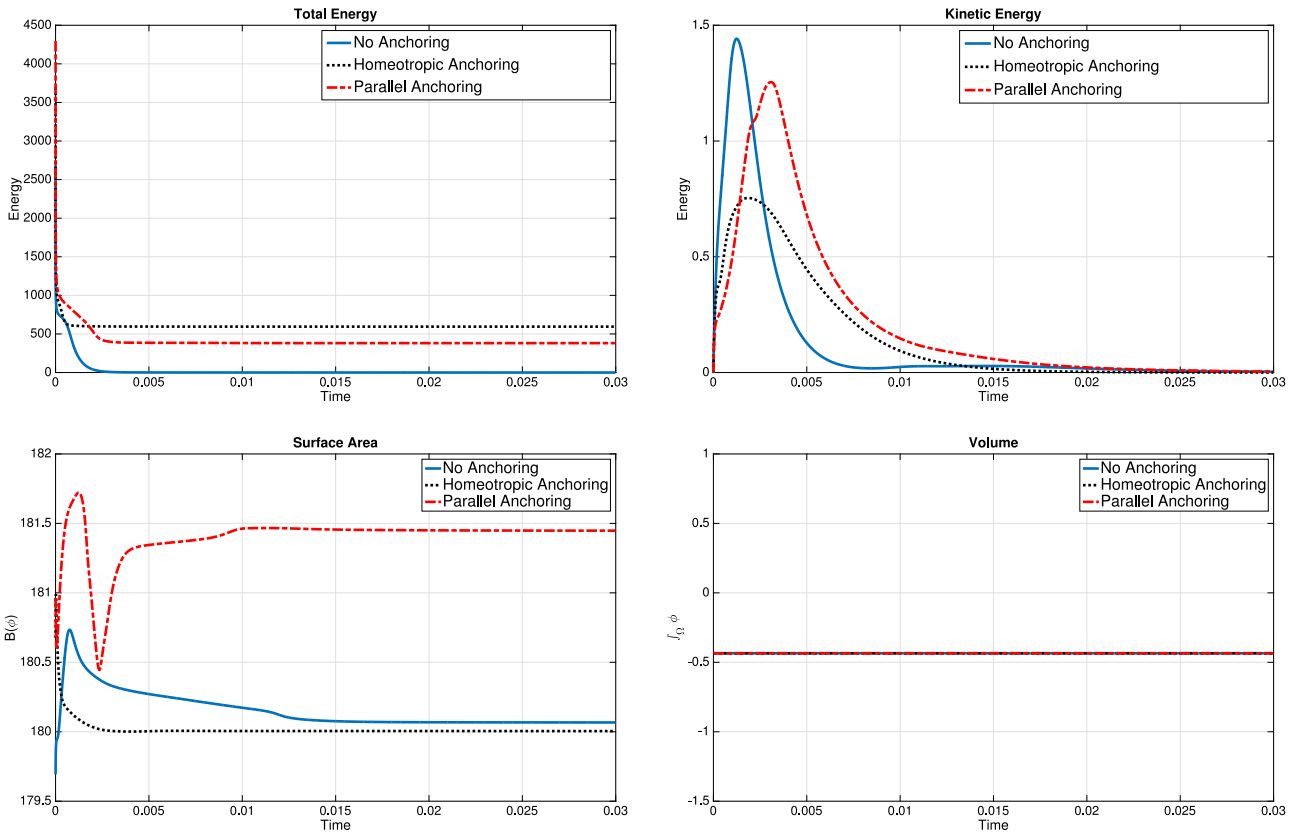


**Fig. 10.** Example III. Results considering vesicles filled with nematic liquid crystal immersed in an isotropic fluid. Top Left: Evolution of Total Energy. Top Right: Evolution of Kinetic Energy. Bottom Left: Evolution of $B(\phi)$. Bottom Right: Evolution of $\int_\Omega \phi$.

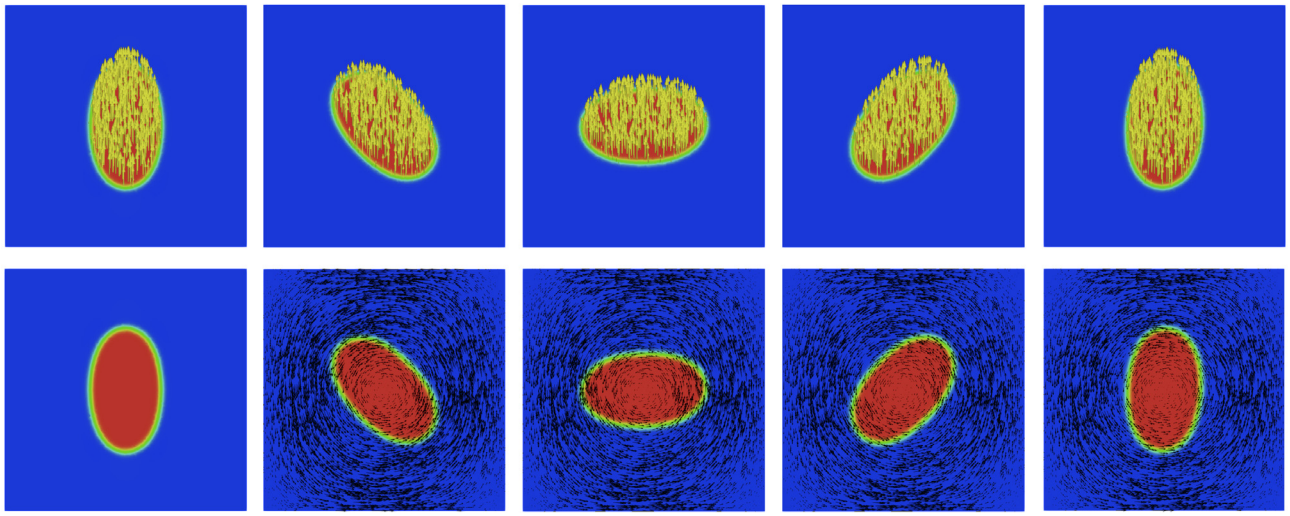

**Fig. 11.** Example IV. Top: Dynamics for a vesicle filled with nematic liquid crystal and immersed in a rotating newtonian fluid at times $t = 0, 0.00006, 0.00012, 0.00018, 0.00024$. Top: $\phi$ (vesicle) and $\boldsymbol{d}$ (nematic liquid crystal orientation). Bottom: $\phi$ (vesicle) and $\boldsymbol{u}$ (fluid).

experience deformation, although the amount of surface (that is, $B(\phi)$) fluctuates a bit (again this fluctuation is related with the fact that we are not imposing the conservation of $B(\phi)$ in an exact way). These results suggest that this model can be considered to perform a more detailed study of the dynamics of vesicles in linear flows, because the rotation of vesicles without deformation are of key importance to capture the dynamics exhibited in the tank-treading and tumbling regimes [7].

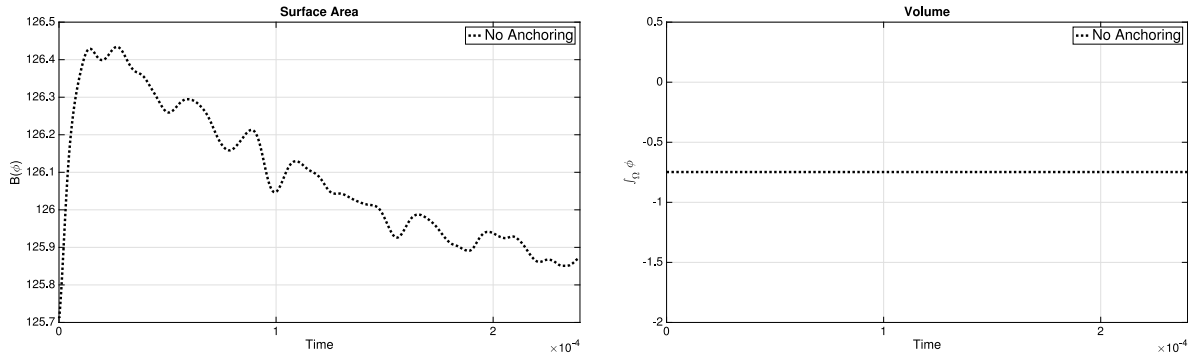


**Fig. 12.** Example VI. Left: Evolution of $B(\phi)$. Right: Evolution of $\int_\Omega \phi$.

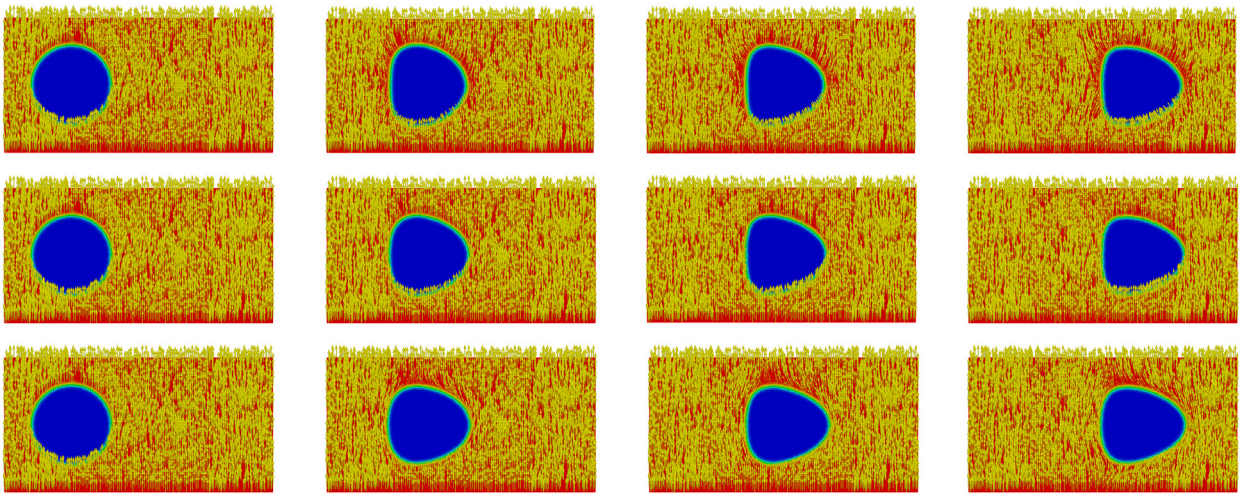

**Fig. 13.** Example V. Dynamics of $\phi$ (vesicle) and $\boldsymbol{d}$ (nematic liquid crystal orientation) for a vesicle filled with an isotropic fluid and immersed in a nematic liquid crystal at times $t = 0, 0.0001, 0.0002, 0.0003$. Initial condition: $\boldsymbol{d} = (0, 1)$. Top: Homeotropic Anchoring ($(\delta_1, \delta_2) = (1, -1)$). Middle: No Anchoring case ($(\delta_1, \delta_2) = (0, 0)$). Bottom: Parallel Anchoring ($(\delta_1, \delta_2) = (0, 1)$).

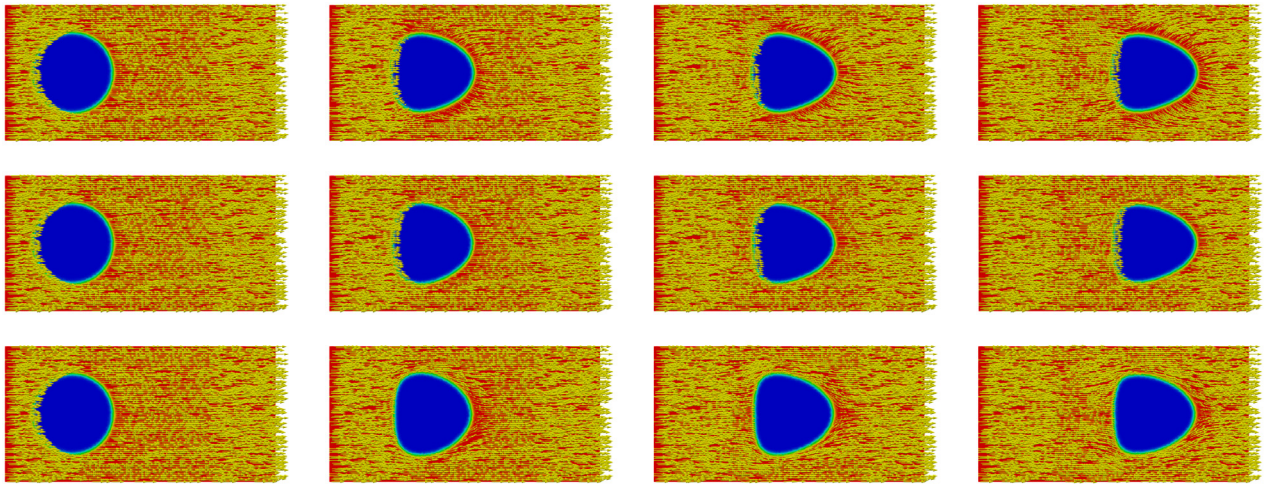

**Fig. 14.** Example V. Dynamics of $\phi$ (vesicle) and $\boldsymbol{d}$ (nematic liquid crystal orientation) for a vesicle filled with an isotropic fluid and immersed in a nematic liquid crystal at times $t = 0, 0.0001, 0.0002, 0.0003$. Initial condition: $\boldsymbol{d} = (1, 0)$. Top: Homeotropic Anchoring ($(\delta_1, \delta_2) = (1, -1)$). Middle: No Anchoring case ($(\delta_1, \delta_2) = (0, 0)$). Bottom: Parallel Anchoring ($(\delta_1, \delta_2) = (0, 1)$).

### 4.5. Example V. Vesicles transported by flow

In this example we study the shapes of vesicles in a two-dimensional Poiseuille flow. The domain considered for this example is a rectangle ($\Omega = [0, 2] \times [0, 1]$), the imposed surface area of the vesicle corresponds with the initial one (that is, $\beta = B(\phi^0)$) and the discrete and physical parameters are the ones presented in Table 4. The initial condition and boundary conditions for the fluid velocity are given by

$$\boldsymbol{u}^0 = (3000 \sin(\pi y), 0), \quad \boldsymbol{u}|_{\partial\Omega_{top}} = \boldsymbol{u}|_{\partial\Omega_{bottom}} = (0, 0) \quad \text{and}$$
$$\boldsymbol{u}|_{\partial\Omega_{left}} = \boldsymbol{u}|_{\partial\Omega_{right}} = (3000 \sin(\pi y), 0).$$

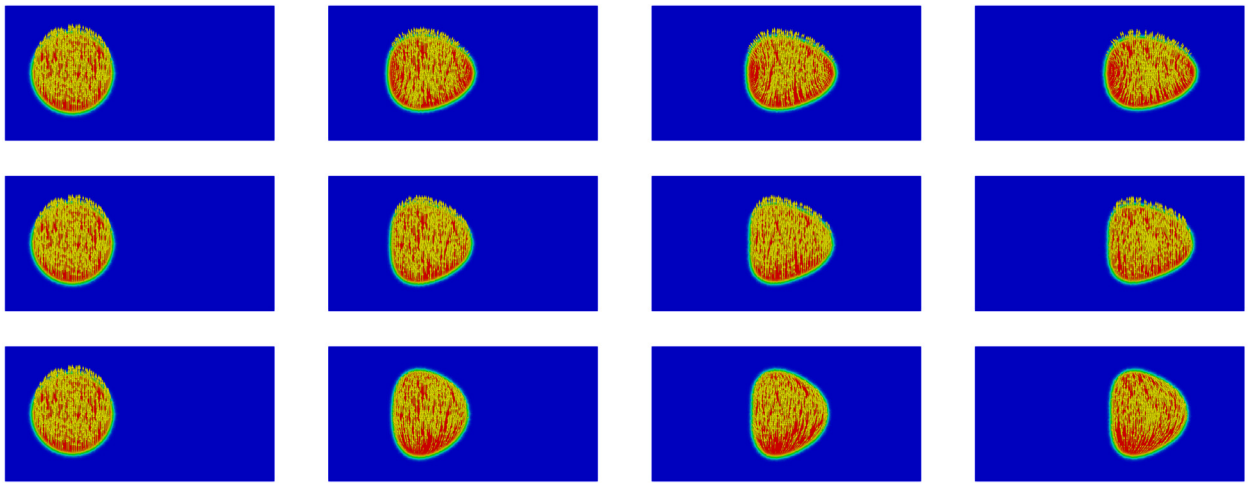

**Fig. 15.** Example V. Dynamics of $\phi$ (vesicle) and $\boldsymbol{d}$ (nematic liquid crystal orientation) for a vesicle filled with nematic liquid crystal immersed in an isotropic fluid with at times $t = 0, 0.0001, 0.0002, 0.0003$. Initial condition: $\boldsymbol{d} = (0, 1)$. Top: Homeotropic Anchoring ($(\delta_1, \delta_2) = (1, -1)$). Middle: No Anchoring case ($(\delta_1, \delta_2) = (0, 0)$). Bottom: Parallel Anchoring ($(\delta_1, \delta_2) = (0, 1)$).

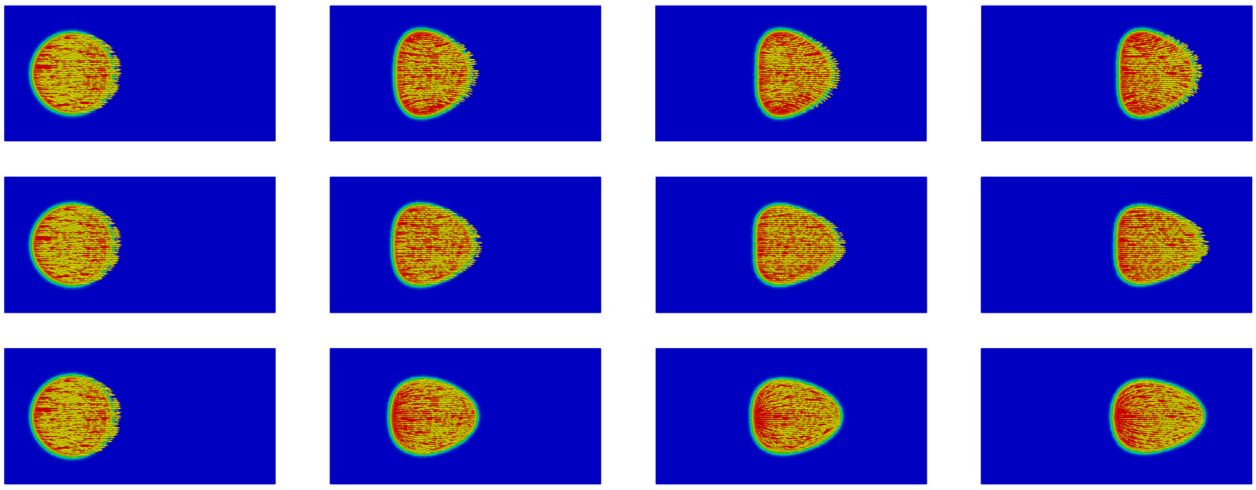

**Fig. 16.** Example V. Dynamics of $\phi$ (vesicle) and $\boldsymbol{d}$ (nematic liquid crystal orientation) for a vesicle filled with nematic liquid crystal immersed in an isotropic fluid with at times $t = 0, 0.0001, 0.0002, 0.0003$. Initial condition: $\boldsymbol{d} = (1, 0)$. Top: Homeotropic Anchoring ($(\delta_1, \delta_2) = (1, -1)$). Middle: No Anchoring case ($(\delta_1, \delta_2) = (0, 0)$). Bottom: Parallel Anchoring ($(\delta_1, \delta_2) = (0, 1)$).

**Table 3**
Parameters considered in Example IV.

| $h$ | $\Delta t$ | $\lambda_{bp}$ | $\lambda_{nem}$ | $\lambda_{anch}$ | $\gamma_{nem}$ | $\gamma_{ben}$ | $\varepsilon$ | $\eta_{\boldsymbol{d}}$ | $\eta$ | $\nu_{Nw}$ | $\nu_{Lc}$ |
|---|---|---|---|---|---|---|---|---|---|---|---|
| 1/100 | $10^{-7}$ | 1.0 | 100.1 | 100.1 | 0.5 | 0.01 | 0.01 | 0.075 | $10^{-5}$ | 1.0 | $10^5$ |

**Table 4**
Parameters considered in Example V.

| $h$ | $\Delta t$ | $\lambda_{bp}$ | $\lambda_{nem}$ | $\lambda_{anch}$ | $\gamma_{nem}$ | $\gamma_{ben}$ | $\varepsilon$ | $\eta_{\boldsymbol{d}}$ | $\eta$ | $\nu_{Nw}$ | $\nu_{Lc}$ |
|---|---|---|---|---|---|---|---|---|---|---|---|
| 1/70 | $10^{-8}$ | 1.0 | 100.1 | 100.1 | 0.5 | 0.01 | 0.01 | 0.075 | $10^{-5}$ | 1.0 | 1.0 |

We have considered two different settings, one where the vesicles are filled with a newtonian fluid and immersed in a nematic liquid crystal and the other where the vesicles are filled with a nematic liquid crystal and immersed in a newtonian fluid. In both settings we have considered two different initial conditions for the orientation of the nematic liquid crystal molecules, namely $\boldsymbol{d}^0 = (0, 1)$ and $\boldsymbol{d}^0 = (1, 0)$. The dynamics of the vesicles immersed in nematic liquid crystal are presented in Figs. 13, 14 while the dynamics of the vesicles immersed in a newtonian fluid are presented in Figs. 15, 16. It can be observed that in the all the cases the vesicles deform to achieve axisymmetric shapes (in particular bullet-like ones) that are different depending on the anchoring effect considered. This type of axisymmetric shapes in the vesicles are expected, because it is known that in a Poiseuille flow, vesicles migrate towards the tip of the flow where the shear rate is minimal, adopting a shape which is symmetric relative to the axis of symmetry of the flow [6]. Interestingly, we can observe how the shape produced by homeotropic anchoring with initial condition $\boldsymbol{d}(0) = (0, 1)$ is the same that the shape achieved in the case of parallel anchoring with initial condition $\boldsymbol{d}(0) = (1, 0)$ and how the shape produced by parallel anchoring with initial condition $\boldsymbol{d}^0 = (0, 1)$ is the same that the shape achieved in the case of homeotropic anchoring case with initial condition $\boldsymbol{d}^0 = (1, 0)$.

### 4.6. Example VI. Vesicles through constrictions

In this section we study the dynamics of vesicles with three different shapes advected by a flow through a constriction. This

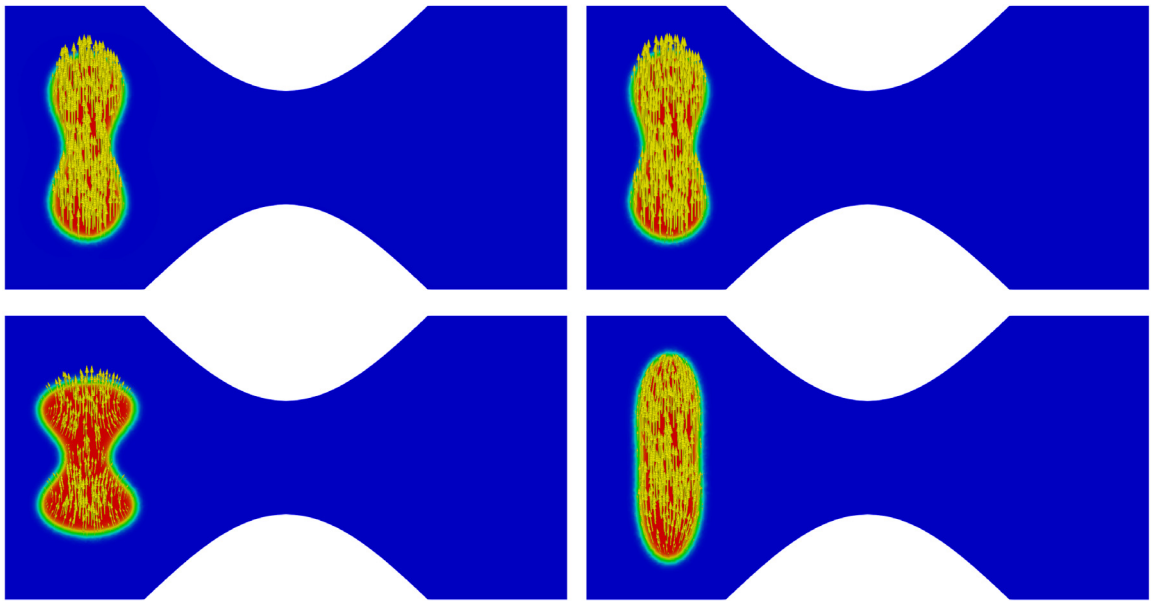

**Fig. 17.** Example VI. Initial and equilibrium configurations for $\phi$ (vesicle) and $\boldsymbol{d}$ (nematic liquid crystal orientation). Top Left: Initial Condition. Top Right: Equilibrium configuration for No Anchoring ($(\delta_1, \delta_2) = (0, 0)$). Bottom Left: Equilibrium configuration for Homeotropic Anchoring ($(\delta_1, \delta_2) = (1, -1)$). Bottom Right: Equilibrium configuration for Parallel Anchoring ($(\delta_1, \delta_2) = (0, 1)$).

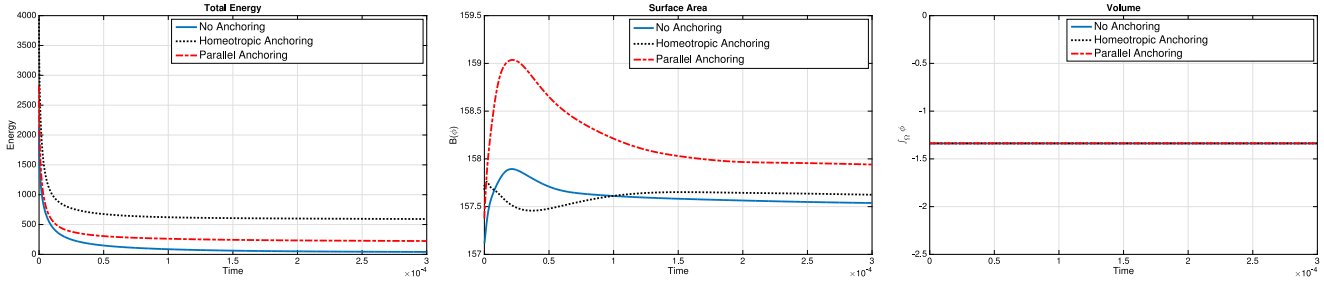


**Fig. 18.** Example VI. Left: Evolution of Total Energy. Center: Evolution of $B(\phi)$. Right: Evolution of $\int_\Omega \phi$. In dashed blue line the No Anchoring case ($(\delta_1, \delta_2) = (0, 0)$), in red dotted line the Homeotropic Anchoring case ($(\delta_1, \delta_2) = (1, -1)$) and in solid black line the Parallel Anchoring case ($(\delta_1, \delta_2) = (0, 1)$).

section is divided into two parts: (1) we start neglecting the fluid part of the system and considering as initial condition a biconcave vesicle with initial orientation of the liquid crystal field $\boldsymbol{d}^0 = (0, 1)$, and we impose the three different types of anchoring effects; (2) we will use the resulting equilibrium configurations from (1) as initial conditions for studying the dynamics of these three different vesicles. Let us remark that the initial configurations of (1) have been computed in the same domain and mesh that is considered for the simulations in (2), in order to avoid difficulties projecting the configurations into different domains/meshes.

*4.6.1. Deformation of a vesicle with anchoring effects and no flow*

In this part of the section we study the influence of the anchoring effects on the equilibrium configurations achieved by the system. The domain considered for this example is a rectangle ($\Omega = [0, 2] \times [0, 1]$) with a narrowing in the middle, the imposed surface area of the vesicle corresponds with the initial one (that is, $\beta = B(\phi^0)$) and the discrete and physical parameters are the ones presented in Table 5.

We carry out simulations using the same initial configuration for $\phi$ and $\boldsymbol{d}$ for each of the possible anchoring effects. In particular, we consider initially $\phi$ as a biconcave cell and $\boldsymbol{d}$ parallel to the $y$-axis ($\boldsymbol{d} = (0, 1)$). Moreover, we consider that there is no flow, in order to isolate the dynamics of the system from the influence of the flow part. The initial condition considered

**Table 5**
Parameters.

| $h$ | $\Delta t$ | $\lambda_{bp}$ | $\lambda_{nem}$ | $\lambda_{anch}$ | $\gamma_{nem}$ | $\gamma_{ben}$ | $\varepsilon$ | $\eta_{\boldsymbol{d}}$ | $\eta$ | $T$ |
|---|---|---|---|---|---|---|---|---|---|---|
| 1/100 | $10^{-7}$ | 1.0 | 100.1 | 100.1 | 0.5 | 0.01 | 0.01 | 0.075 | $10^{-5}$ | $3 \times 10^{-4}$ |

for the three cases and the obtained equilibrium configurations are presented in Fig. 17 and the evolution of the energies and the approximation of the constraints are presented in Fig. 18. We can observe how the obtained equilibrium configurations are different in each case, with the homeotropic anchoring moving $\boldsymbol{d}$ and deforming the vesicle in such a way that the orientation of $\boldsymbol{d}$ is perpendicular to mostly all the membrane while the shape of the membrane tries to minimize the curvature. The parallel anchoring also moves $\boldsymbol{d}$ and deform the membrane but in this case to obtain a configuration where the orientation of $\boldsymbol{d}$ is parallel to mostly all the membrane while the shape of the membrane tries to minimize the curvature. Meanwhile, the no anchoring case does not produce any visible change on the configuration of $\boldsymbol{d}$ or $\phi$, because the initial condition is already in a shape that minimizes the curvature. In the three cases the total energy of the system is decreasing in time as expected. Interestingly, in all of the dynamics there is a small readjustment of the surface area of the vesicle, which is not too surprising due to the fact that the system is minimizing a total energy (2.5) with contributions

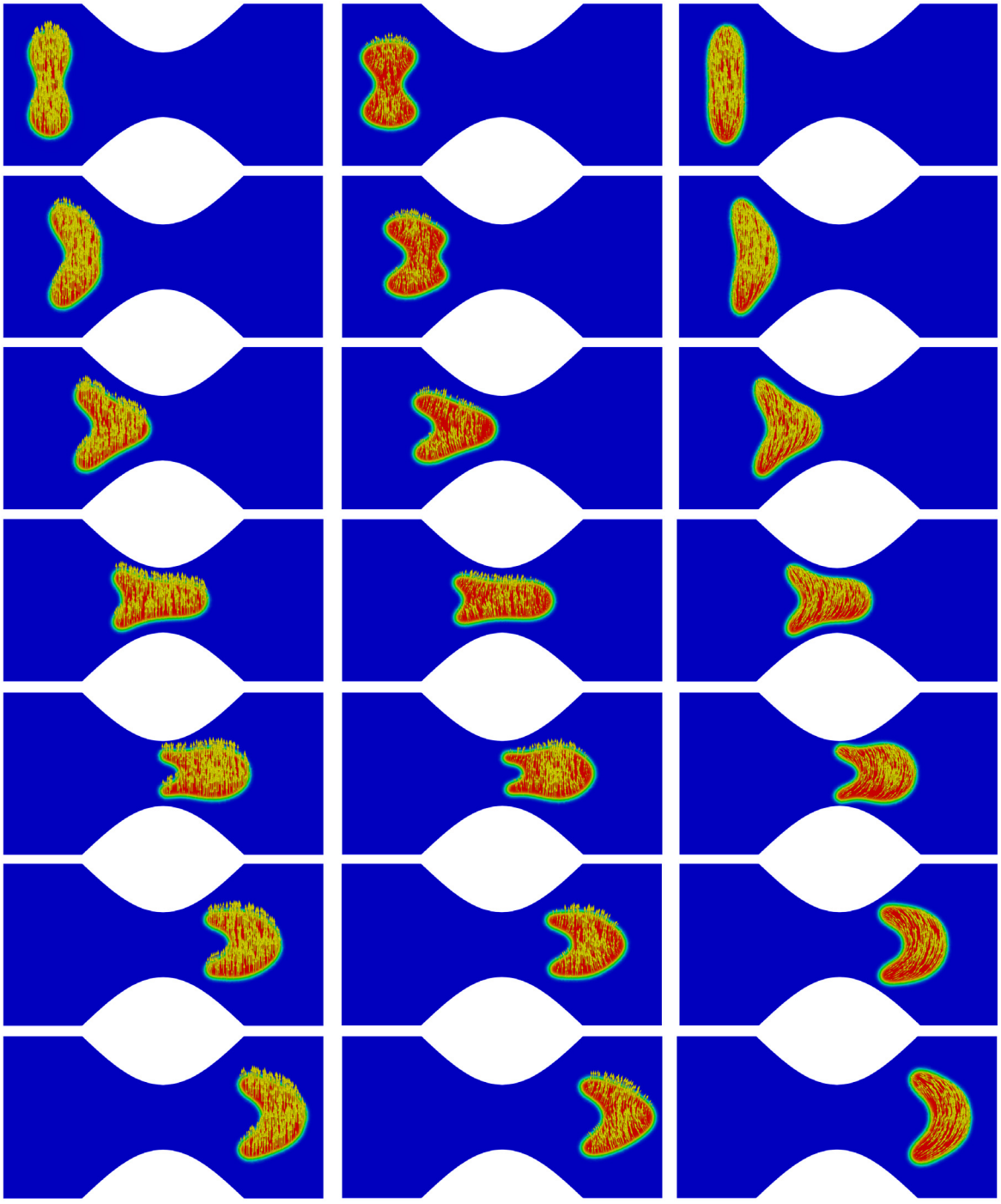

**Fig. 19.** Example VI. Dynamics of $\phi$ (vesicle) and $\boldsymbol{d}$ (nematic liquid crystal orientation) for vesicles transported by flow at times $t = 0, 0.00006, 0.00012, 0.00018, 0.00024, 0.0003, 0.00036$ (from Top to Bottom). Left: No Anchoring ($(\delta_1, \delta_2) = (0, 0)$). Center: Homeotropic Anchoring ($(\delta_1, \delta_2) = (1, -1)$). Right: Parallel Anchoring ($(\delta_1, \delta_2) = (0, 1)$).

from different effects and under the considered weights ($\lambda_{nem} = \lambda_{anch} \gg \lambda_{bp}$) the system focus on minimizing the nematic and anchoring part instead of the bending part. Obviously, changes in the values of $\lambda_{bp}$, $\lambda_{nem}$, $\lambda_{anch}$ will lead to completely different dynamics and probably to different equilibrium configurations.

*4.6.2. Deformation and advection of vesicles filled with liquid crystal by a isotropic flow in a channel with a narrowing in the middle*

Now we study the dynamics of vesicles advected by a flow in a channel with a narrowing where the vesicles have to deform in order to go through the narrowing trying to maintain the volume and the imposed surface area. We consider as initial conditions the equilibrium configurations obtained in Section 4.6.1 (see Fig. 17). The flow is a Poiseuille-like flow, that is we are considering:

$$\boldsymbol{u}^0 = \boldsymbol{u}|_{\partial\Omega_{Left}} = \boldsymbol{u}|_{\partial\Omega_{Right}} = (3000\sin(\pi y), 0),$$
$$\boldsymbol{u}|_{\partial\Omega_{Top}} = \boldsymbol{u}|_{\partial\Omega_{Bottom}} = (0, 0)$$

and

$$\nu_{Nw} = \nu_{Lc} = 1.0.$$

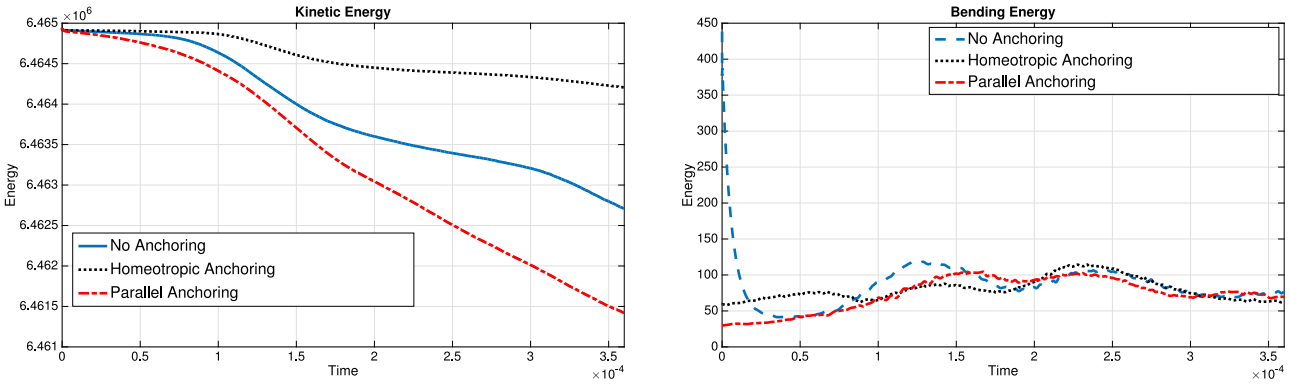


**Fig. 20.** Example VI. Left: Evolution of Kinetic Energy. Right: Evolution of Bending Energy. In dashed blue line the No Anchoring case ($(\delta_1, \delta_2) = (0, 0)$), in red dotted line the Homeotropic Anchoring case ($(\delta_1, \delta_2) = (1, -1)$) and in solid black line the Parallel Anchoring case ($(\delta_1, \delta_2) = (0, 1)$).

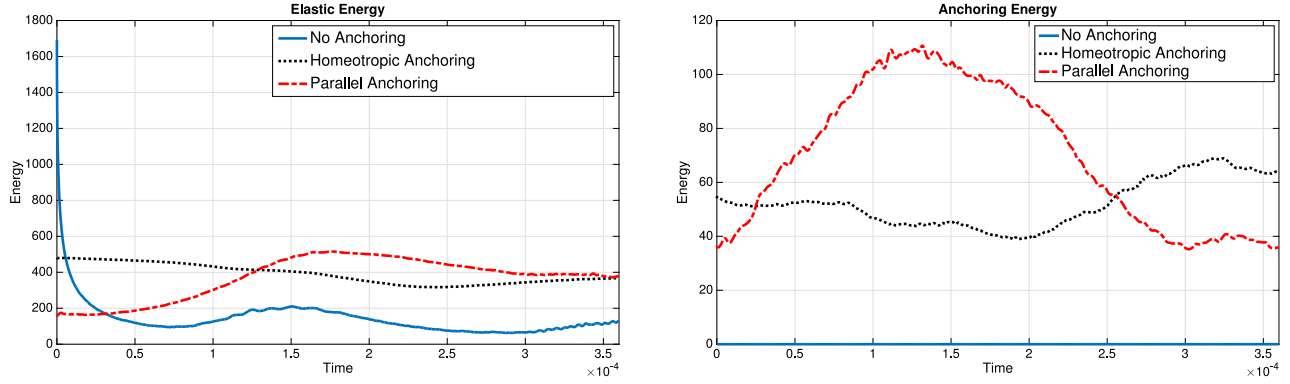


**Fig. 21.** Example VI. Left: Evolution of Elastic Energy. Right: Evolution of Anchoring Energy. In dashed blue line the No Anchoring case ($(\delta_1, \delta_2) = (0, 0)$), in red dotted line the Homeotropic Anchoring case ($(\delta_1, \delta_2) = (1, -1)$) and in solid black line the Parallel Anchoring case ($(\delta_1, \delta_2) = (0, 1)$).

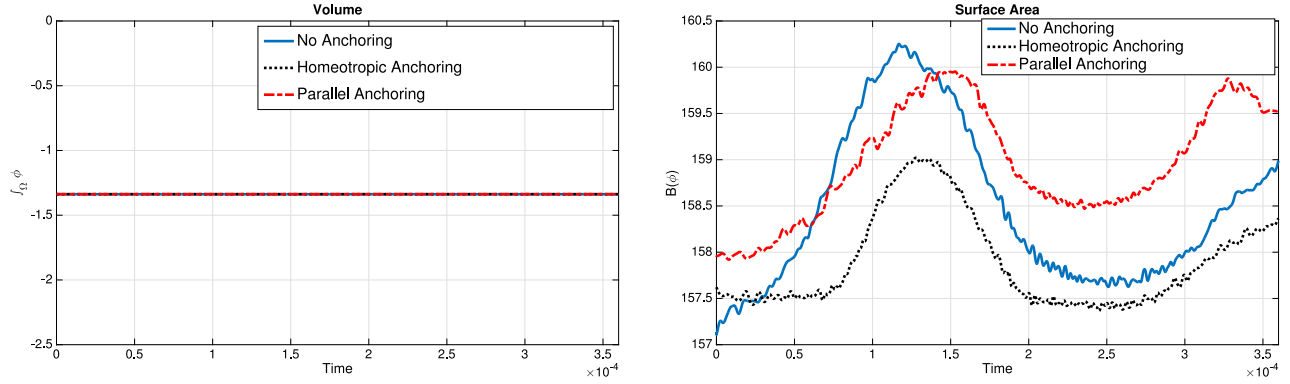


**Fig. 22.** Left: Evolution of $\int_\Omega \phi$. Right: Evolution of $B(\phi)$. In dashed blue line the No Anchoring case ($(\delta_1, \delta_2) = (0, 0)$), in red dotted line the Homeotropic Anchoring case ($(\delta_1, \delta_2) = (1, -1)$) and in solid black line the Parallel Anchoring case ($(\delta_1, \delta_2) = (0, 1)$).

The dynamics of the three cases are presented in Fig. 19, the kinetic and bending energies of the systems are plotted in Fig. 20 and the nematic and anchoring energies of the systems are plotted in Fig. 21. Moreover the evolution in time of $\int_\Omega \phi$ and $B(\phi)$ are presented in Fig. 22. We can observe that in the three cases the vesicles exhibit deformation in order to be transported through the narrowing and this fact produces changes in the surface area of the vesicles ($B(\phi)$). In fact, after the vesicles go through the narrowing, they deform themselves to a new parachute-like configuration that keep the original surface area value. The parachute-like shape is well known to appear when working with vesicles in Poiseuille flows [6]. Again, the weight of the different parts of the energy ($\lambda_{bp}$, $\lambda_{nem}$, $\lambda_{anch}$) determine the dynamics of the system, and different sets of parameters will lead to different dynamics. Moreover we can observe that $\int_\Omega \phi$ (a quantity directly related with the volume of the vesicles) always remains constant (as expected). It is interesting to note in the case of considering parallel anchoring, the deformation of the vesicle through the narrowing produces the system to reconfigure itself in such a way that the orientation of the nematic molecules in

the interface is very different from being parallel to the interface, and this fact produces an increase in the anchoring energy, as can be observed in Fig. 21.

## 5. Conclusions

In this paper we have studied a system that can be used to represent vesicle membranes immersed in a newtonian fluid with internal nematic order as well as to represent vesicle membranes filled with isotropic fluid and immersed in a nematic liquid crystal. Firstly, taking into account kinetic, bending, nematic and anchoring effects we have derived a thermodynamically consistent model that includes the contributions of all the effects. Then, we have derived a splitting numerical scheme that allows us to split the computation of the unknowns in three different sub-steps (reducing the computational cost when compared with a coupled scheme), computing first the nematic part $(\boldsymbol{d}, \boldsymbol{z})$ (director vector-equilibrium), then computing the vesicle part $(\phi, \mu, \omega)$ (phase field variables) and finally the fluid part $(\boldsymbol{u}, p)$ (velocity–pressure).

We have reported the results of several numerical simulations using the presented new numerical scheme, showing that the numerical scheme is efficient and accurate, achieving energy-stability in all the cases where no external forces are applied to the system. Moreover, we have demonstrated how the interaction of the vesicle with the nematic liquid crystal (independently that if the liquid crystal is inside or outside the vesicle) influences the achievable shape configurations of the vesicle. Additionally, the proposed numerical scheme is able to capture interesting features exhibited by vesicles in experiments such as rotation of the vesicles in rotating fluids, deformation through constrictions and axisymmetric shapes when the vesicles are transported by Poiseuille flows.

Finally, the obtained results suggest that the presented numerical scheme is a good choice to try to addressed interesting questions by doing a systematically study of the possible dynamics and equilibrium configurations that vesicles can exhibit, due to its efficiency and accuracy. In fact, because the proposed system is energy-stable, it can be viewed (when no external forces are applied) as a way of finding minima (or at least critical points) of the non-convex energy functional. A systematic study of the minima will provide a better understanding of the possible equilibrium shapes that vesicles can exhibit. In fact, this model and the numerical scheme can be used in 3$D$ domains, and the splitting character of the scheme makes it a better choice from the computational point of view than any coupled scheme. Moreover, another interesting set of questions are related with the interactions with flows, and it will be interesting to study in detail some of the effects described in the nice review [6], like tumbling, tank-treading, elongational flow or even to obtain phase diagrams of vesicles in Poiseuille flows as a function of the reduced volume and the maximal flow velocity.

## Declaration of competing interest

The authors declare that they have no known competing financial interests or personal relationships that could have appeared to influence the work reported in this paper.

## Acknowledgments

This research work has been supported by *Proyecto PGC2018-098308-B-I00*, financed by FEDER/Ministerio de Ciencia e Innovación - Agencia Estatal de Investigación, Spain.

## References

[1] R.A. Barrio, T. Alarcon, A. Hernandez-Machado, The dynamics of shapes of vesicle membranes with time dependent spontaneous curvature, PLoS One 15 (2020) e0227562.
[2] F. Campelo, A. Hernández-Machado, Shape instabilities in vesicles: A phase-field model, Eur. Phys. J. Spec. Top. 143 (2007) 101–108.
[3] F. Campelo, A. Cruz, J. Pérez-Gil, L. Vázquez, A. Hernández-Machado, Phase-field model for the morphology of monolayer lipid domains, Eur. Phys. J. E 35 (2012) 49.
[4] S. Hocine, A. Brulet, J. Lin, J. Yang, A. Di Cicco, L. Bouteillerce, M.H. Li, Structural changes in liquid crystal polymer vesicles induced by temperature variation and magnetic fields, Soft Matter 7 (2011) 2613–2623.
[5] D. Barthes-Biesel, Motion and deformation of elastic capsules and vesicles in flow, Annu. Rev. Fluid Mech. 48 (2016) 25–52.
[6] D. Abreu, M. Levant, V. Steinberg, U. Seifert, Fluid vesicles in flow, Adv. Colloid Interface Sci. 208 (2014) 129–141.
[7] B. Kaoui, J. Harting, Two-dimensional lattice Boltzmann simulations of vesicles with viscosity contrast, Rheol. Acta 55 (2016) 465–475.
[8] R. Kusters, T.van.der. Heijden, B. Kaoui, J. Harting, C. Storm, Forced transport of deformable containers through narrow constrictions, Phys. Rev. E 90 (2014) 033006.
[9] A. Le Goff, B. Kaoui, G. Kurzawa, B. Haszon, A.V. Salsac, Squeezing biocapsules into a constriction: deformation till break-up, Soft Matter. 13 (2017) 7644.
[10] T.S. Nguyen, J. Geng, R.L.B. Selinger, J.V. Selinger, Nematic order on a deformable vesicle: theory and simulation, Soft Matter. 9 (2013) 8314.
[11] L.T. Tan, N.L. Abbott, Dynamic anchoring transitions at aqueous-liquid crystal interfaces induced by specific and non-specific binding of vesicles to proteins, J. Colloid Interface Sci. 449 (2015) 452–461.
[12] R. Zhang, Y. Zhou, M. Rahimi, J.J. de Pablo, Dynamic structure of active nematic shells, Nature Commun. 7 (2016) 13483.
[13] Y. Bouligand, Liquid crystals and biological morphogenesis: Ancient and new questions, C. R. Chim. 11 (2008) 281–296.
[14] P. Rofouie, D. Pasini, A.D. Rey, Morphology of elastic nematic liquid crystal membranes, Soft Matter 13 (2017) 5366.
[15] R. Zhang, Y. Zhou, J.A. Martinez-Gonzalez, J.P. Hernandez-Ortiz, N.L. Abbott, J.J. de Pablo, Controlled deformation of vesicles by flexible structured media, Sci. Adv. 2 (8) (2016) e1600978.
[16] F.C. Keber, E. Loiseau, T. Sanchez, S.J. DeCamp, L. Giomi, M.J. Bowick, M.C. Marchetti, Z. Dogic, A.R. Bausch, Topology and dynamics of active nematic vesicles, Science 345 (2014) 1135–1139.
[17] X. Xing, H. Shin, M.J. Bowick, L. Yao, M.H. Li, Morphology of nematic and smectic vesicles, Proc. Natl. Acad. Sci. USA 109 (2012) 5202–5206.
[18] M.M. Genkin, A. Sokolov, O.D. Lavrentovich, I.S. Aranson, Topological defects in a living nematic ensnare swimming bacteria, Phys. Rev. X 7 (2017) 011029.
[19] S. Zhou, A. Sokolov, O.D. Lavrentovich, I.S. Aranson, Living liquid crystals, Proc. Natl. Acad. Sci. USA 111 (4) (2014) 1265–1270.
[20] S. Zhou, O. Tovkach, D. Golovaty, A. Sokolov, I.S. Aranson, O.D. Lavrentovich, Dynamic states of swimming bacteria in a nematic liquid crystal cell with homeotropic alignment, New J. Phys. 19 (2017) 055006.
[21] J. Beaucourt, F. Rioual, T. Séon, T. Biben, C. Misbah, Steady to unsteady dynamics of a vesicle in a flow, Phys. Rev. E 69 (2004) 011906.
[22] T. Biben, K. Kassner, C. Misbah, Phase-field approach to three-dimensional vesicle dynamics, Phys. Rev. E 72 (2005) 041921.
[23] T. Biben, C. Misbah, Tumbling of vesicles under shear flow within an advected-field approach, Eur. Phys. J. B 29 (2002) 311–316.
[24] T. Biben, C. Misbah, Tumbling of vesicles under shear flow within an advected-field approach, Phys. Rev. E 67 (2003) 031908.
[25] T. Biben, C. Misbah, A. Leyrat, C. Verdier, An advected-field approach to the dynamics of fluid interfaces, Europhys. Lett. 63 (2003) 623–629.
[26] Q. Du, C. Liu, R. Ryham, X. Wang, Energetic variational approaches in modeling vesicle and fluid interactions, Physica D 238 (2009) 923–930.
[27] Q. Du, C. Liu, X. Wang, A phase field approach in the numerical study of the elastic bending energy for vesicle membranes, J. Comput. Phys. 198 (2004) 450–468.
[28] Q. Du, C. Liu, X. Wang, Simulating the deformation of vesicle membranes under elastic bending energy in three dimensions, J. Comput. Phys. 212 (2006) 757–777.
[29] Q. Du, X. Wang, Convergence of numerical approximations to a phase field bending elasticity model of membrane deformations, Int. J. Numer. Anal. Model. 4 (2007) 441–459.
[30] T. Banham, B. Li, Y. Zhao, Pattern formation by phase-field relaxation of bending energy with fixed surface area and volume, Phys. Rev. E 90 (3) (2014) 033308.
[31] B. Climent-Ezquerra, F. Guillén-González, Convergence to equilibrium of global weak solutions for a Cahn–Hilliard–Navier–Stokes vesicle model, Z. Angew. Math. Phys. 70 (2019) 125.

[32] Q. Du, M. Li, C. Liu, And analysis of a phase field navier-stokes vesicle-fluid interaction model, Discrete Contin. Dyn. Syst. 8 (2007) 539–556.
[33] R. Chen, G. Ji, X. Yang, H. Zhang, And decoupled energy stable schemes for phase-field vesicle membrane model, J. Comput. Phys. 302 (2015) 509–523.
[34] Q. Du, J. Zhang, Adaptive finite element method for a phase field bending elasticity model of vesicle membrane deformations, SIAM J. Sci. Comput. 30 (2008) 1634–1657.
[35] Q. Du, L. Zhu, Analysis of a mixed finite element method for a phase field bending elasticity model of vesicle membrane deformation, J. Comput. Math. 24 (2006) 265–280.
[36] L.T. Gao, X.Q. Feng, H. Gao, A phase field method for simulating morphological evolution of vesicles in electric fields, J. Comput. Phys. 228 (2009) 4162–4181.
[37] F. Guillén-González, G. Tierra, Unconditionally energy stable numerical schemes for phase-field vesicle membrane model, J. Comput. Phys. 354 (2018) 67–85.
[38] F.E. Mackay, C. Denniston, Deformable vesicles interacting in a nematic liquid crystal, Soft Matter. 9 (2013) 5285.
[39] F. Ziebert, I.S. Aranson, Computational approaches to substrate-based cell motility, npj, Comput. Mater. 2 (2016) 16019.
[40] F. Guillén-González, M.A. Rodríguez-Bellido, G. Tierra, Nematic order on a deformable vesicle with anchoring effects, Results Appl. Math. 8 (2020) 100102.
[41] F. Guillén-González, M.A. Rodríguez-Bellido, G. Tierra, Linear unconditional energy-stable splitting schemes for a phase-field model for nematic-isotropic flows with anchoring effects, Internat. J. Numer. Methods Engrg. 108 (2016) 535–567.
[42] Q. Du, C. Liu, R. Ryham, X. Wang, Phase field modeling of the spontaneous curvature effect in cell membranes, Commun. Pure Appl. Anal. 4 (2005) 537–548.
[43] F. Campelo, A. Hernández-Machado, Dynamic model and stationary shapes of fluid vesicles, Eur. Phys. J. E 20 (2006) 37–45.
[44] P. Yue, J.J. Feng, C. Liu, J. Shen, A diffuse-interface method for simulating two-phase flows of complex fluids, J. Fluid Mech. 515 (2004), 293–317.
[45] J.J. Feng, C. Liu, J. Shen, P. Yue, An energetic variational formulation with phase field methods for interfacial dynamics of complex fluids: advantages and challenges, in: Modeling of Soft Matter, Springer, New York, 2005, pp. 1–26.
[46] C. Liu, H. Sun, On energetic variational approaches in modeling the nematic liquid crystal flows, Discrete Contin. Dyn. Syst. A 23 (2009), 455–475.
[47] Y. Hyon, D.Y. Kwak, C. Liu, Energetic variational approach in complex fluids: maximum dissipation principle, Discrete Contin. Dyn. Syst. A 26 (2010) 1291–1304.
[48] G. Tierra, J.P. Pavissich, R. Nerenberg, Z. Xu, M.S. Alber, Multicomponent model of deformation and detachment of a biofilm under fluid flow, J. R. Soc. Interface 12 (2015) 20150045.
[49] S. Xu, Z. Xu, O.V. Kim, R.I. Litvinov, J.W. Weisel, M.S. Alber, Model predictions of deformation, embolization and permeability of partially obstructive blood clots under variable shear flow, J. R. Soc. Interface 14 (2017) 20170441.
[50] V. Girault, P.A. Raviart, Finite Element Methods for Navier–Stokes Equations: Theory and Algorithms, Springer-Verlag, Berlin, 1986.
[51] G. Tierra, F. Guillén-González, Numerical methods for solving the cahn-hilliard equation and its applicability to related energy-based models, Arch. Comput. Methods Eng. 22 (2015) 269–289.
[52] F. Guillén-González, G. Tierra, On linear schemes for a cahn hilliard diffuse interface model, J. Comput. Phys. 234 (2013) 140–171.
[53] F. Guillén-González, G. Tierra, Second order schemes and time-step adaptivity for Allen–Cahn and Cahn–Hilliard models, Comput. Math. Appl. 68 (2014) 821–846.
[54] F. Hecht, New development in FreeFem++, J. Numer. Math. 20 (2012) 251–265.